Original Article

MOLECULAR METABOLISM

Sex-specific metabolic functions of adipose Lipocalin-2

Karthickeyan Chella Krishnan [1,*], Simon Sabir [2], Michaël Shum [3], Yonghong Meng [1], Rebeca Acín-Pérez [3], Jennifer M. Lang [1], Raquel R. Floyd [4], Laurent Vergnes [5], Marcus M. Seldin [1], Brie K. Fuqua [1], Dulshan W. Jayasekera [6], Sereena K. Nand [4], Diana C. Anum [7], Calvin Pan [1], Linsey Stiles [3], Miklós Péterfy [1,8], Karen Reue [5], Marc Liesa [3,9], Aldons J. Lusis [1,5,6,*]

ABSTRACT

Objective: Lipocalin-2 (LCN2) is a secreted protein involved in innate immunity and has also been associated with several cardiometabolic traits in both mouse and human studies. However, the causal relationship of LCN2 to these traits is unclear, and most studies have examined only males.

Methods: Using adeno-associated viral vectors we expressed LCN2 in either adipose or liver in a tissue specific manner on the background of a whole-body *Lcn2* knockout or wildtype mice. Metabolic phenotypes including body weight, body composition, plasma and liver lipids, glucose homeostasis, insulin resistance, mitochondrial phenotyping, and metabolic cage studies were monitored.

Results: We studied the genetics of LCN2 expression and associated clinical traits in both males and females in a panel of 100 inbred strains of mice (HMDP). The natural variation in *Lcn2* expression across the HMDP exhibits high heritability, and genetic mapping suggests that it is regulated in part by *Lipin1* gene variation. The correlation analyses revealed striking tissue dependent sex differences in obesity, insulin resistance, hepatic steatosis, and dyslipidemia. To understand the causal relationships, we examined the effects of expression of LCN2 selectively in liver or adipose. On a *Lcn2*-null background, LCN2 expression in white adipose promoted metabolic disturbances in females but not males. It acted in an autocrine/paracrine manner, resulting in mitochondrial dysfunction and an upregulation of inflammatory and fibrotic genes. On the other hand, on a null background, expression of LCN2 in liver had no discernible impact on the traits examined despite increasing the levels of circulating LCN2 more than adipose LCN2 expression. The mechanisms underlying the sex-specific action of LCN2 are unclear, but our results indicate that adipose LCN2 negatively regulates its receptor, LRP2 (or megalin), and its repressor, ERα, in a female-specific manner and that the effects of LCN2 on metabolic traits are mediated in part by LRP2.

Conclusions: Following up on our population-based studies, we demonstrate that LCN2 acts in a highly sex- and tissue-specific manner in mice. Our results have important implications for human studies, emphasizing the importance of sex and the tissue source of LCN2.

Keywords Sex differences; Diet-induced obesity; Insulin resistance; Adipose fibrosis; Adipose inflammation; Mitochondrial dysfunction

1. INTRODUCTION

Lipocalin-2 (LCN2), also known as neutrophil gelatinase-associated lipocalin (NGAL), is a secreted glycoprotein that was first studied in human neutrophils [1,2]. LCN2's role in innate immunity against gram-negative bacteria has been thoroughly investigated and is well known for its binding and sequestering of bacterial siderophores (bacterial iron scavenging molecules), thereby restricting iron from the bacteria and implementing nutritional immunity [3,4]. Over the years, several investigators have shown that other cells such as adipocytes [5,6], hepatocytes [7,8], renal tubular cells [9,10], and, more recently, bone osteoblasts [11] can also secrete LCN2 in various disease states, expanding the functional roles of LCN2. In the context of metabolism, LCN2 has been implicated in several cardio-metabolic disease states including obesity, inflammation and insulin resistance [5,6,11–17], alcoholic and non-alcoholic fatty liver disease [18,19], cardiac hypertrophy, heart failure, and atherosclerosis [20–22]. However, most of these animal studies have used only males from a single genetic background (C57BL/6J) with limited studies investigating their female counterparts. Added to that, whole body knockout (rather than tissue-specific knockout) animal models were mostly used, making it difficult to interpret the specific source for these associations. Similarly, only

[1]Department of Medicine/Division of Cardiology, University of California, Los Angeles, CA, USA [2]Department of Psychology, University of California, Los Angeles, CA, USA [3]Department of Medicine/Division of Endocrinology, University of California, Los Angeles, CA, USA [4]Department of Biology, University of California, Los Angeles, CA, USA [5]Department of Human Genetics, University of California, Los Angeles, CA, USA [6]Department of Microbiology, Immunology and Molecular Genetics, University of California, Los Angeles, CA, USA [7]Department of Integrative Biology and Physiology, University of California, Los Angeles, CA, USA [8]Department of Basic Medical Sciences, Western University of Health Sciences, Pomona, CA, USA [9]Department of Molecular and Medical Pharmacology, University of California, Los Angeles, CA, USA

*Corresponding author. UCLA, Department of Medicine/Division of Cardiology, 650 Charles E. Young Drive South, Box 951679, Los Angeles, CA, 90095-1679, USA. E-mails: kchellakrishnan@mednet.ucla.edu (K. Chella Krishnan), JLusis@mednet.ucla.edu (A.J. Lusis).

Received July 22, 2019 • Revision received September 4, 2019 • Accepted September 22, 2019 • Available online 27 September 2019

https://doi.org/10.1016/j.molmet.2019.09.009

serum LCN2 levels were used to examine associations in human studies [13,14,23,24].

Our specific focus in this study was to investigate the role of LCN2 in diet-induced animal models of obesity and to examine the potential involvement of gene-by-sex interactions. To this end, we used the Hybrid Mouse Diversity Panel (HMDP) that consists of both sexes from >100 classical inbred and recombinant inbred mouse strains. These animals were fed a diet containing high fat and high sucrose (HF/HS) for eight-weeks to study obesity [25], insulin resistance [26,27], gut microbial composition [28,29], and non-alcoholic fatty liver disease [30–33]. We observed striking sex-specific, gonadal hormone-mediated regulation of adipose *Lcn2* expression. Our results are consistent with previous studies showing that LCN2 has a role in estradiol production and estrogen signaling [34] and that the estrogen receptor ERα indeed binds to the adipose *Lcn2* promoter and represses *Lcn2* expression [35]. Using *in vivo* animal models, we demonstrate that adipose-secreted, and not liver-secreted, LCN2 is causal in developing diet-induced metabolic complications, but only in females. Mechanistically, we show that high levels of adipose LCN2 induce mitochondrial dysfunction and increased inflammation- and fibrosis-related gene signatures in adipose tissue only in females. Explaining the sex difference, transcriptomics data revealed that LCN2 acts through the female-specific negative regulation of its receptor, megalin (LRP2), and its repressor, estrogen receptor (ER)α.

2. METHODS

2.1. Ethics statement

All animal studies were performed in strict accordance with the recommendations in the Guide for the Care and Use of Laboratory Animals of the National Institutes of Health. All of the animals were handled according to approved institutional animal care and use committee (IACUC) protocols (#92-169) of the University of California at Los Angeles and were housed in an IACUC-approved vivarium with daily monitoring by vivarium personnel.

2.2. Animals

The HMDP study design was previously described in detail [25,26]. Briefly, the animals were fed ad libitum a chow diet (Ralston Purina Company) until 8 weeks of age and then placed ad libitum on a high fat/high sucrose (HF/HS) diet (Research Diets-D12266B, New Brunswick, NJ) with 16.8% kcal protein, 51.4% kcal carbohydrate, 31.8% kcal fat for an additional 8 weeks (total 16 weeks of age). The gonadectomy study design was previously described in detail [26]. Briefly, at 6 weeks of age, female and male C57BL/6J mice were either gonadectomized or sham-operated under isoflurane anesthesia and placed on a HF/HS diet around 8 weeks of age. All mice including the *Lcn2*-null mice (B6.129P2- *Lcn2*^{tm1Aade}/AkiJ) on C57BL/6J background and C57BL/6J wildtype (WT) mice were purchased from The Jackson Laboratory and bred at University of California, Los Angeles. Mice were maintained on a 14 h light/10 h dark cycle (light is on between 6 a.m. and 8 p.m.). On the day of the experiment, the mice from both studies were sacrificed after 4-hour fasting.

2.3. RNA isolation

Flash-frozen gonadal adipose samples upon sacrifice were weighed and homogenized in QIAzol (Qiagen, Germantown, MD), and following chloroform phase separation, RNA was isolated according to the manufacturer's protocol using miRNeasy columns (Qiagen, Germantown, MD).

2.4. HMDP adipose gene expression analysis

Global gene expression was analyzed for the isolated RNA using Affymetrix HT_MG430A arrays and microarray data was filtered as previously described [36]. Then, ComBat method from the SVA Bioconductor package [37] was used to remove known batch effects on the gene expression data.

2.5. Library preparation and sequencing

Libraries were prepared from extracted gonadal fat RNA (Agilent 2200 Tapestation eRIN >8.2) using KAPA Stranded mRNA-Seq Kit (cat #KK8421, KAPA Biosystems, Wilmington, MA), per the manufacturers' instructions. The pooled libraries were sequenced with an Illumina HiSeq4000 instrument, SE50bp reads (Illumina, San Diego, CA). Reads were aligned to the mouse genome mm10 using STAR [38] or HISAT2 [39] aligner and quantified using the Bioconductor R packages as described in the RNA-Seq workflow [40]. *P* values were adjusted using the Benjamini-Hochberg procedure of multiple hypothesis testing [41].

2.6. Transcript-phenotype correlations

For every pairwise combination between phenotypes and gonadal *Lcn2* expression, in each sex, we calculated biweight midcorrelation (a robust, and not sensitive to outliers, alternative to Pearson correlation) using bicorAndPvalue function of the WGCNA package [42].

2.7. Tissue deconvolution analyses

Cell type composition of adipose tissue was analyzed using gene expression data by deconvolution with SaVanT (http://newpathways.mcdb.ucla.edu/savant-dev) using cell type signatures from the Human Primary Cell Atlas. Cell-type signature score refers to the average of gene expression values of top 50 genes for the respective signature-sample combination. The greater the signature score, the higher the proportion of the respective cell population within the sample.

2.8. Adeno-associated virus generation

For overexpression studies, recombinant adeno-associated virus serotype 8 (AAV8) expressing LCN2 or GFP was generated as described previously [43,44]. Briefly, mouse *Lcn2* cDNA or GFP was cloned into an AAV expression plasmid under an adiponectin promoter (AAV8-hAdp) with a liver-specific miRNA target sequence (miR122T) for adipose-specific expression [44] or a thyroxine binding globulin (AAV8-Tbg) promoter for liver-specific expression. To generate deficiency models, we knockdown *Lrp2* using the AAV8-hAdp-miR122T vector expressing shRNA sequences. Efficacious shRNAs were identified and experimentally verified *in vitro*, as follows. The top 10 shRNA sequences predicted [45] for each candidate gene were cloned into an optimized miRNA scaffold (shRNAmir) [46] driven by the ubiquitous H1 promoter and cotransfected with luciferase-target gene fusion constructs into HEK293 cells. Knockdown efficiency were evaluated using luciferase reporter assays, and the most effective shRNAmir was subcloned into the AV8-hAdp-miR122T vector. Viral packaging, propagation, and purification were carried out at the University of Pennsylvania Gene Therapy program vector core.

2.9. LCN2 overexpression and LRP2 knockdown studies

Eight-week old female and male *Lcn2*-null mice or female WT mice were injected intravenously with either adipose-specific or liver-specific AAV containing LCN2 or GFP constructs for overexpression or

adipose-specific AAV containing shRNA against *ffLuc* or *Lrp2* for knockdown studies (10^{12} titer in 200 μL saline). A day after the injection, the animals were placed on HF/HS diet for an additional 8- or 16-weeks. Body composition (fat and lean mass) was determined using NMR (Brüker Biospin Corp, Billerica, MA). On the day of the sacrifice, the animals were fasted for 4 h, followed by their sacrifice and tissue extraction. Retro-orbital blood was collected to isolate plasma for analyzing glucose, insulin and lipids; liver tissues were collected for lipid content analyses; four white adipose depots (gonadal, subcutaneous, mesenteric and retroperitoneal) and brown adipose were collected for weight measurements. The HOMA-IR was calculated using the equation $[(Glucose\ X\ Insulin)/16903]$. Liver lipids were extracted as described previously [47]. Briefly, lipids extracted from about 60 mg of liver were dissolved in 1.8% (wt/vol) Triton X-100, and colorimetric assays from Sigma (St. Louis, MO) (triglyceride, total cholesterol and unesterified cholesterol) and Wako (Richmond, VA) (phospholipids) were performed according to the manufacturer's instructions.

2.10. *Ex vivo* 3T3-L1 antisense oligonucleotide (ASO) treatment

Mouse 3T3-L1 cells were cultured in preadipocyte medium (Zenbio Inc.). Cells were reverse transfected with Lipofectamine RNAiMAX (Invitrogen) and a control or lipin-1 antisense oligonucleotide (Ionis Pharmaceutical Inc.) [48]. After 2 days, cells were harvested in Trizol reagent to isolate total RNA.

2.11. *Ex vivo* iWAT and poWAT LCN2 treatment

The inguinal (iWAT) or periovarian (poWAT) white preadipocytes were isolated from the stromal vascular fraction of inguinal or periovarian white adipose from 8 weeks old female *Lcn2*-null mice, respectively. The pre-iWAT or pre-poWAT cells were maintained in Dulbecco's Modified Eagle Medium: Nutrient Mixture F-12 (DMEM/F12) supplemented with 1% glutamax, 10% fetal calf serum and 100 U/ml of both penicillin and streptomycin (basal media). Two days after plating (day 0), when the cells reached nearly 100% confluency, the cells were treated with an induction media containing basal media supplemented with 4 μg/mL insulin, 0.5 mM IBMX, 1 μM dexamethasone, and 1 μM rosiglitazone. After 48 h, the cells were treated with a maintenance media containing the basal media supplemented with 4 μg/mL insulin, and 1 μM rosiglitazone, with a media change every 2 days until day 10. For qPCR, differentiated iWAT cells were treated with 1 μg/ml recombinant LCN2 (Sino Biological Inc.) for 24 h after which RNA was collected. For bioenergetics, 5×10^4 differentiated poWAT cells were plated in XF-24 seahorse plate treated with 1 μg/ml recombinant LCN2 (Sino Biological Inc.) for 24 h after which oxygen consumption rates were measured.

2.12. Quantitative polymerase chain reaction

Total RNA was isolated from frozen mouse gonadal adipose tissues or iWAT cells using QIAzol (Qiagen, Germantown, MD) following manufacturer's RNA isolation protocol. First-strand complementary DNA (cDNA) was made from 2 μg total RNA of each mouse according to the manufacturer's protocol using High-Capacity cDNA Reverse Transcription Kit (Applied Biosystems, Waltham, MA). Relative quantitative gene expression levels were measured by quantitative PCR using Kapa SYBR Fast qPCR kit (Kapa Biosystems, Inc., Wilmington, MA) on a LightCycler 480 II (Roche) and analyzed using the Roche LightCycler1.5.0 Software. The geometric mean of B2M and TBP was used to normalize all qPCR targets [49]. Relative normalized expression was measured using the equation $2^{-\Delta\Delta Ct}$. All qPCR primer sequences were listed below.

Gene	Sequence 5′ to 3′
B2m	Forward: TACGTAACACAGTTCCACCCGCCTC
	Reverse: GCAGGTTCAAATGAATCTTCAGAGCATC
Tbp	Forward: CAAACCCAGAATTGTTCTCCTT
	Reverse: ATGTGGTCTTCCTGAATCCCT
Ccl2	Forward: TTAAAAACCTGGATCGGAACCAA
	Reverse: GCATTAGCTTCAGATTTACGGGT
Lcn2	Forward: ACGGACTACAACCAGTTCGC
	Reverse: AATGCATTGGTCGGTGGGG
Lrp2	Forward: AAAATGGAAACGGGGTGACTT
	Reverse: GGCTGCATACATTGGGTTTTCA
Esr1	Forward: GCCAGAATGGCCGAGAGAG
	Reverse: CCCCATAATGGTAGCCAGAGG
Polg1	Forward: TAGCTGGCTGGTCCAAGAGT
	Reverse: CGACGTGGAGGTCTGCTT

2.13. Immunoblot analyses

Animal tissues and cultured cells were homogenized using RIPA buffer containing protease and phosphatase inhibitors. Samples were then separated by SDS-PAGE, transferred to PVDF membranes and probed using the following antibodies: LCN2 (R&D Systems, AF1857), LRP2 (abcam, ab76969), ERα (abcam, ab32063), β-ACTIN (Cell Signaling, 4967L), GAPDH (Invitrogen, PA1-987) and Vinculin (Sigma, V9131).

2.14. Glucose- and insulin-tolerance tests

For glucose- and insulin-tolerance tests, mice were fasted for 6 h, unless reported otherwise, and then challenged with an intraperitoneal injection of glucose (1 g/kg) and insulin (1 U/kg), respectively. Blood glucose levels were monitored using the AlphaTRAK blood glucose monitoring system (Zoetis, Parsippany, NJ) at times indicated.

2.15. Metabolic cages

Indirect calorimetry was performed using a Columbus Instruments Comprehensive Lab Animal Monitoring System (CLAMS, Columbus Instruments). Animals were placed individually in chambers for 3 consecutive days at ambient temperature (26.5 °C) with 12 h light/dark cycles. Animals had free access to food and water. Respiratory measurements were made in 20 min intervals after initial 7–9 h acclimation period. Energy expenditure was calculated from VO_2 and RER using the Lusk equation, EE in Kcal/hr = (3.815 + 1.232 X RER) X VO2 in ml/min. Food intake was measured in metabolic chambers. Body composition (fat and lean mass) was determined using EchoMRI Body Composition Analyzer.

2.16. Mitochondrial DNA content

Mitochondrial DNA content was measured as described previously [50–52]. Briefly, total (mitochondrial and nuclear) DNA from gonadal adipose tissue was isolated by phenol/chloroform/isoamyl alcohol extraction. Both mitochondrial and nuclear DNA were amplified by quantitative PCR with 25 ng of total DNA using primers in the D-loop region (AATCTACCATCCTCCGTGAAACC; TCAGTTTAGCTACCCCCAAGTTTAA) and Tert gene (CTAGCTCATGTGTCAAGACCCTCTT; GCCAGCACGTTTCTCTCGTT), respectively. Mitochondrial DNA content, normalized to nuclear DNA, was calculated using the equation $2\ X\ 2^{-\Delta Ct}$ (ΔCt = D-loop Ct −Tert Ct) and then reported as relative units of corresponding GFP groups.

2.17. Bioenergetics of isolated mitochondria

Isolated mitochondrial respiration from adipose tissue [53] were measured as described previously. Briefly, mitochondria were obtained by dual centrifugation and resuspended in respiration buffer [53] and kept on

ice. Mitochondrial respiration from different complexes was obtained with an XF24 Seahorse bioanalyzer (Agilent). For electron flow assays, basal OCR was measured in presence of 10 mM pyruvate (Complex I substrate), 2 mM malate and 4 mM FCCP, and after sequential addition of 2 mM rotenone (Complex I inhibitor), 10 mM succinate (Complex II substrate), 4 mM antimycin A (Complex III inhibitor) and 1 mM TMPD containing 10 mM ascorbate (Complex IV substrate). Complex III respiration corresponds to the antimycin A-sensitive respiration.

2.18. Mitochondrial immunoblot procedures and analyses of function

Adipose mitochondria (10–20 μg) prepared for mitochondria bioenergetics as described above were re-suspended in NuPAGE LDS Sample Buffer with protease inhibitor cocktail and incubated at 45 °C for 10 min. Samples were then loaded into 4%–12% Bis-Tris precast gels (Thermo Fisher Scientific NP0321) and electrophoresed in xCell SureLock (Novex) in constant voltage at 60 V for 15 min (to clear stacking) and 150 V for 45 min. Proteins were transferred to methanol-activated PVDF membrane in xCell SureLock in 30 V constant voltage for 1 hr at 4 °C. Blots were blocked with 5% non-fat dry milk in PBST (1 mL/L Tween-20/PBS) and incubated with primary antibodies to Complex I (NDUFB8, Thermo Fisher Scientific #459210), Complex II (SDHB, Abcam #175225), Complex III (UQCRC1, Thermo Fisher Scientific #459140), Complex IV (COX4, Thermo Fisher Scientific #459600), ATP Synthase (ATP5A1, Thermo Fisher Scientific #43-9800) and TOM20 (Santa Cruz, #11415) diluted in 1% BSA/PBST overnight at 4 °C. The next day, blots were washed in PBST, probed with HRP-linked secondary antibodies diluted in blocking solution for 1 hr at room temperature, and rinsed again in PBST. Detection was achieved by ECL-Plus reagent and imaging was performed with Typhoon 9410 Molecular Imager (Amersham). Image contrast was uniformly reduced to enhance visibility. Band densitometry was quantified using ImageJ Gel Plugin (NIH).

2.19. Cellular bioenergetics

5×10^4 differentiated poWAT cells seeded in a XF24 plate treated with recombinant LCN2 for 24 h were analyzed in a XF24 analyzer (Agilent) as described [54]. Briefly, oxygen consumption rates (OCR) were measured before and after the sequential injections of 0.75 mM oligomycin, 2 mM FCCP, and 0.75 mM of rotenone/myxothiazol. Mixing, waiting, and measurement times were 3, 2, and 3 min, respectively. Measures were normalized by total protein.

2.20. Data availability

RNA sequencing raw data can be accessed at the Gene Expression Omnibus (GEO) under accession GSE121098.

2.21. Statistical analysis

Statistical analyses were performed using Prism v7.0a (GraphPad Software, Inc., La Jolla, CA, USA). Errors bars plotted on graphs are presented as the mean ± SEM unless reported otherwise. The critical significance value (α) was set at 0.05, and if the P values were less than α, we reported that, by rejecting the null hypothesis, the observed differences were statistically significant.

3. RESULTS

3.1. Genetics- and sex-specific regulation of adipose and liver *Lcn2* expression and its association with metabolic traits

To investigate the effects of genetics and sex on gene expression in a tissue-specific manner, we investigated the expression profiles from adipose and liver tissues of ~100 age- and sex-matched mouse strains (HMDP) fed a HF/HS diet. As seen in Figure 1A, among several well-known sexually dimorphic autosomal genes in adipose such as *Sult1e1* [55] and *Ucp1* [56–58], *Lcn2* stood out as one of the most strongly and significantly downregulated genes in female adipose (~7-fold F < M, P = 1.9E-30; Figure 1A,C). In striking contrast, *Lcn2* expression was significantly upregulated in female livers (~2-fold F > M, P = 1.1E-09; Figure 1B,E). Individual matched-strain expression profiles shown in Supplementary Figure S1 revealed both genetic and sex-specific control. Also, as shown in Supplementary Figure S2, plasma LCN2 levels increased in C57BL/6J females when fed a HF/HS diet suggesting a pathophysiological relevance to our study. To further characterize the role of sex hormones, follow-up RNASeq studies involving gonadectomized C57BL/6J mice (Figure 1D,F) revealed that ovariectomy in females lead to the loss of estrogen-dependent adipose *Lcn2* repression [35] while gonadectomy in males lead to the upregulation of liver *Lcn2* repression. In contrast, no significant differences were observed between sham-treated and gonadectomized males in adipose expression albeit with large variance between individual males (Figure 1D), and between sham-treated and gonadectomized females in liver expression (Figure 1F).

Next, we interrogated the HMDP populations to test for any strong sex-specific association(s) between adipose or liver *Lcn2* expression and clinically significant metabolic traits. Figure 1G shows that female, but not male, adipose *Lcn2* expression was strongly and positively (1% FDR cutoff) associated with metabolic traits such as obesity, tissue weights, dyslipidemia, insulin resistance and steatosis. Surprisingly, we observed only a few weak associations between female liver *Lcn2* expression and metabolic traits, while stronger but few associations were observed in males (Figure 1H). Individual bicorrelation coefficients and *P* values for each association are listed in Supplementary Table S1. Taken together, these results support the concept that adipose *Lcn2* contributes to dysregulation of metabolic traits in females and liver *Lcn2* may contribute to dysregulation of male traits, specifically insulin resistance.

3.2. Genetic control of *Lcn2* expression: identification of *Lpin1* as a potential *trans*-regulator gene

Lcn2 expression varies substantially among the HMDP strains in adipose as well as liver and in both sexes (Supplementary Figure S1). This is due in large part to genetics and heritability of *Lcn2* transcript levels is high except in male adipose (female adipose = 0.647 ± 0.059; male adipose = 0.075 ± 0.048: female liver = 0.358 ± 0.089: male liver = 0.281 ± 0.076), Given this, we next searched for genetic loci that significantly control *Lcn2* expression in a tissue-by-sex specific manner.

Association mapping of *Lcn2* expression revealed a female adipose-specific *trans*-acting expression quantitative trait locus (eQTL) on chromosome 12 and a female-specific *trans*-acting eQTL on chromosome 15 (Supplementary Figure 3a). High-resolution regional plots of these two loci revealed *Lpin1* and *Ntsr2* in chr12 and *6030458C11Rik* in chr15 as potential candidate genes regulating *Lcn2* expression (Supplementary Figure 3b). These candidate genes were identified based on three criteria: i) they had strong *cis*-eQTL in their respective tissues, ii) their respective peak *cis*-SNPs are in strong linkage disequilibrium (LD) with *Lcn2 trans*-SNPs, and iii) their expression is strongly correlated with *Lcn2* expression. To determine if these genes are independently regulating female adipose *Lcn2* expression, association mapping was repeated, but this time we conditioned on *Lpin1* or *Ntsr2* or *6030458C11Rik* expression. Conditioning on *Lpin1* expression suppressed both loci, while the other two

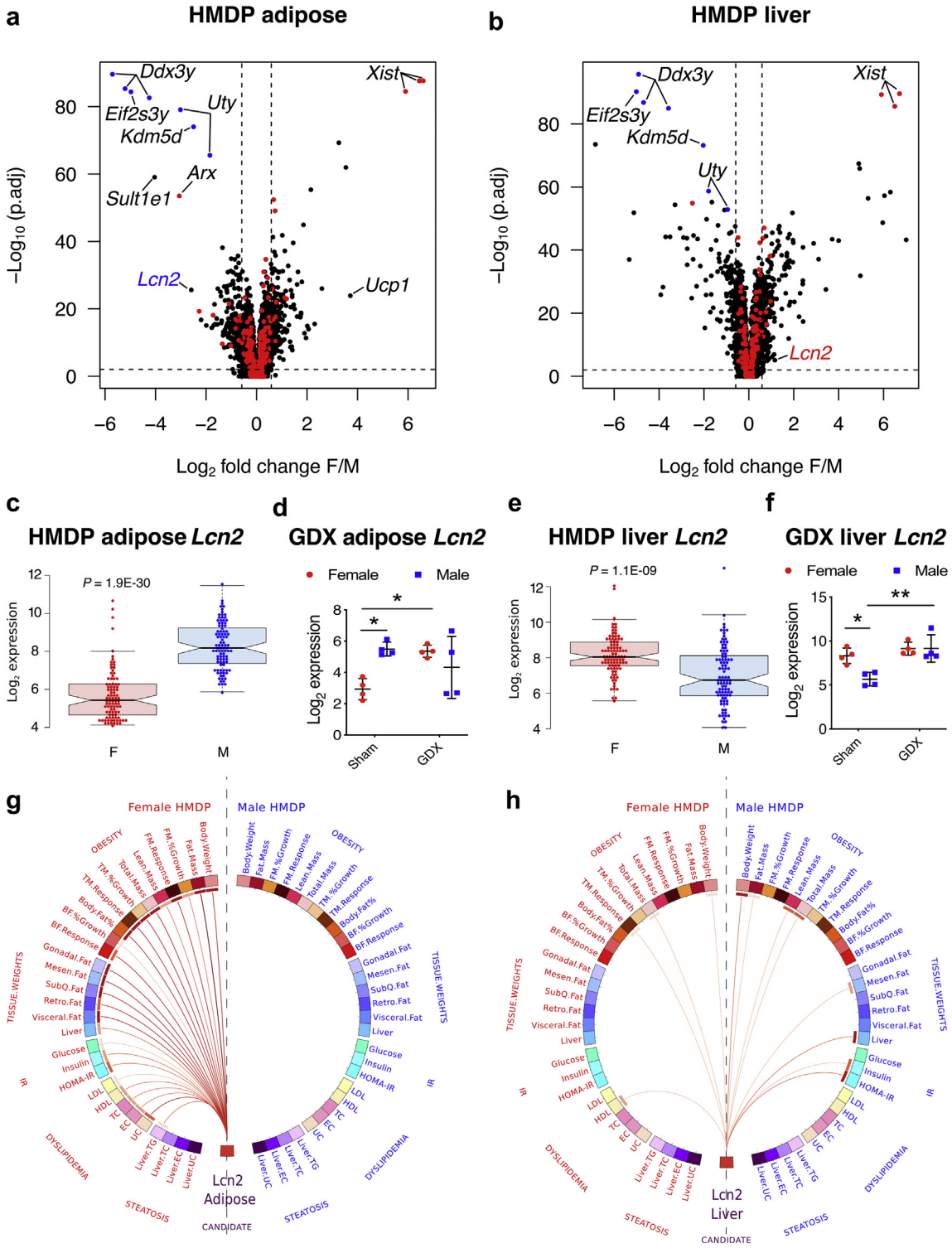

Figure 1: *Lcn2* expression in liver and adipose is highly sexually dimorphic and exhibits sex-specific associations with metabolic traits in the HMDP population, Volcano plots showing sex differences in gene expression profiles from **A,** adipose and **B,** liver tissues isolated from age- and sex-matched mouse strains (HMDP). The red and blue dots represent X and Y chromosomal genes, respectively. Average *Lcn2* expression in female (red) and male (blue) **C,** adipose and **E,** liver tissues from each strain in the HF/HS fed HMDP cohort (n = 98 sex-matched strains with 2–4 mice per sex/strain). **D,** Adipose and **F,** liver *Lcn2* expression in intact and gonadectomized C57BL/6J mice of both sexes (n = 4 per group). Red for females and blue for males. Circos connectogram plot showing biweight midcorrelation between **G,** adipose or **H,** liver *Lcn2* expression and metabolic traits in female and male HMDP cohort (n = 102 female and 111 male strains). Each connecting line signify a significant (1% FDR cutoff) bicorrelation between *Lcn2* expression and the respective trait. Red line indicates positive correlation and the color intensity signify the magnitude of correlation. Data are presented as **A and B,** $\log_2$ fold change (F/M); **C and E,** median and interquartile range; **D and F,** mean ± SEM and **G and H,** midweight bicorrelation. *P* values (and Q values for RNA sequencing data) were calculated by **A and B,** DESeq function of Bioconductor R-package for RNA sequencing; **C and E,** Unpaired Student's t test; **D and F,** 2-factor ANOVA corrected by post-hoc "Holm-Sidak's" multiple comparisons test; **G and H,** BicorAndPvalue function of the WGCNA R-package. $^*P < 0.05$; $^{**}P < 0.01$. See also Figures S1–S2 and Table S1.

genes either suppressed only one locus and/or introduced new loci (Supplementary Figure 3c). Further, the correlation structure between these genes and *Lcn2* expression revealed *Lpin1* as a strong negative regulator of female adipose *Lcn2* expression (Supplementary Figure 3d). *Lpin1* gene encodes the protein lipin-1, a Mg^{2+}-dependent phosphatidate phosphatase type-1 (PAP1) enzyme, which catalyzes the conversion of phosphatidate to diacylglycerol, precursor for triacylglycerol and other glycerolipids [59]. Mice with natural mutations in the *Lpin1* gene exhibit fatty liver dystrophy characterized by loss of body fat, fatty liver and insulin resistance [60]. Two alternatively-spliced isoforms of lipin-1 have been identified that play a distinct role in either adipose differentiation or lipogenesis, respectively [61]. Further, lipin-1 physically interacts with peroxisome proliferator-activated receptor γ2 (PPARγ2) and enhances its activity by recruiting other coactivators [62]. More specifically to this paper, lipin-1 interacts with nuclear factor of activated T cells c4 (NFATc4) repressing its activity and inhibiting adipokine secretions [63]. As a proof of concept, we used antisense oligonucleotide (ASO)-mediated silencing of *Lpin1* [48] in 3T3-L1 preadipocytes and observed a significant increase in *Lcn2* expression levels (Supplementary Figure 3e). Our results suggest that lipin-1 controls *Lcn2* expression although further investigations are warranted to understand the underlying mechanism.

3.3. Adipose LCN2 alters obesity, plasma lipids, insulin resistance, and hepatic steatosis in females

To functionally validate the causal role of adipose LCN2 in metabolic traits, we expressed either LCN2 or green fluorescent protein (GFP) in adipose tissues of 8-week old *Lcn2*-null mice of both sexes and fed them a HF/HS diet for 8 additional weeks. Adipose-specific LCN2 expression (Supplementary Figure 4) was achieved by using adeno-associated viral serotype-8 (AAV8) vectors harboring both adiponectin promoter/enhancer elements and miR122 target sequences (AAV8-hAdp-GFP-miR122T or AAV-hAdp-LCN2-miR122T). AAV8 vectors have specific tropism for liver, heart and adipose, and to some extent in CNS, muscle, pancreas, lung, testis, and kidney [44,64]. The adiponectin promoter/enhancer elements restrict the expression to adipose and liver and not heart, muscle, lung, kidney, and pancreas [44]. To ensure the adipose tissue specificity of LCN2 expression and exclude liver expression, the microRNA122 target sequence at the 3' end results in selective degradation if LCN2 driven by the adiponectin promoter is expressed in the liver [44] (Supplementary Figure 5). We observed a significant increase in total body weight of adipose LCN2 overexpressing females (Figure 2A) likely due to increased fat mass (Figure 2C), while lean mass remained unaltered (Figure 2B). Consequently, the body fat percentage increases (Figure 2D). LCN2 overexpression in adipose tissue also led to a significant increase in tissue weights of liver and white adipose depots compared with the control groups (Figure 2E). However, the BAT of both sexes was not affected by adipose LCN2 overexpression (Figure 2F). All these sex-specific differences were observed despite similar upregulation of plasma LCN2 in both sexes (Figure 2E,F).

Previous studies using male *Lcn2*-null mice reported conflicting results, ranging from LCN2 playing a minor role [16] to protective [15] to potentiating [17] high fat diet-induced insulin resistance. More recently, bone-derived LCN2 was shown to regulate glucose homeostasis in males [11]. Our adipose-specific LCN2 overexpression studies revealed increased insulin resistance in females as indicated by higher fasting plasma glucose, insulin and HOMA-IR values (Figure 2G). Accordingly, glucose tolerance tests revealed that adipose LCN2 overexpression in females led to increased glucose intolerance (Supplemental Figure S6a). Supporting the concept that glucose intolerance was associated with worsened insulin resistance, insulin levels measured after 30 min of glucose administration were higher (Supplemental Figure S6b). In contrast to females, overexpression of adipose LCN2 in males improved glucose metabolism without affecting the body weight (Figure 2H and Supplemental Figure S6c and S6d). We also noted a significant increase in plasma levels of total cholesterol (TC), unesterified cholesterol (UC) and HDL cholesterol levels in females but not in males (Figure 2I,J). Moreover, liver lipid measurements showed hepatic triglyceride (TG) accumulation, a measure of steatosis, to be significantly increased in females (Figure 2I) but not in males (Figure 2J).

These dramatic effects of AAV-mediated overexpression of LCN2 in female adipose, namely obesity and metabolic complications, are not observed under normal conditions due to repression of *Lcn2* expression through ERα-estradiol signaling. Our AAV strategy circumvents this ERα-mediated repression. Thus, when we compared female littermates of *Lcn2*-null and heterozygous mice that were fed a HF/HS diet for 8-weeks we did not observe any body weight differences (Supplementary Figure S7).

3.4. Liver LCN2 is a reactive protein in response to diet-induced obesity

To examine the effects of liver-derived LCN2, we expressed LCN2 or GFP in liver tissues of *Lcn2*-null mice using AAV8 vectors under a thyroxine binding globulin (Tbg) promoter (AAV8-Tbg-GFP or AAV8-Tbg-LCN2). Surprisingly, we did not observe any significant metabolic changes in either sex, despite substantial levels of LCN2 overexpression in both liver and circulation (Supplemental Figures S5, S8 and S9). Although liver-specific overexpression of LCN2 resulted in a greater increase in circulating LCN2 levels than did adipose overexpression (Figure 2E,F; Supplemental Figure. S8e and S8f), only adipose-derived LCN2 caused metabolic complications in females.

One important question relates to the difference between the liver- and adipose-derived LCN2. Song et al., demonstrated that LCN2 is post-translationally modified by polyamination that aids in its rapid clearance from circulation [65]. However, adipose-derived LCN2 from high fat diet-fed mice is predominantly in the non-polyaminated form, while the liver-derived LCN2 is not, and the non-polyaminated form plays a causal role in cardiometabolic traits [65,66]. They also demonstrate that incubating recombinant LCN2 with adipose tissues ($\geq$16hr incubation) from LCN2KO mice resulted in removal of polyamination [65]. Further, the same group demonstrated that adipose-derived LCN2 can also mediate both acute and chronic renal injuries and that this is independent of kidney-derived LCN2 [67]. In contrast, cell-type-resolved liver proteomics revealed that LCN2 is predominantly secreted by Kupffer cells (hepatic macrophages) and not the hepatocytes, implying that increased LCN2 expression in the liver signifies an inflammatory environment in response to obesity [68]. This may explain why our liver LCN2 overexpression in hepatocytes did not cause any metabolic changes in these mice. Altogether, these results indicate a sex-specific autocrine/paracrine (local) role for adipose LCN2 and a lack of impact of circulating LCN2 produced in liver.

3.5. Long term adipose LCN2-mediated metabolic complications

To exclude any bias associated in generating *Lcn2*-null mice and to explore long-term effects of adipose LCN2 overexpression, we fed female C57BL/6J wildtype (WT) mice overexpressing either GFP or LCN2 in adipose tissues with HF/HS diet for a total of 16-weeks. The animals were not subjected to any intervention for the first 8-weeks and then underwent several metabolic tests including glucose tolerance test (GTT), insulin tolerance test (ITT) and indirect calorimetry as

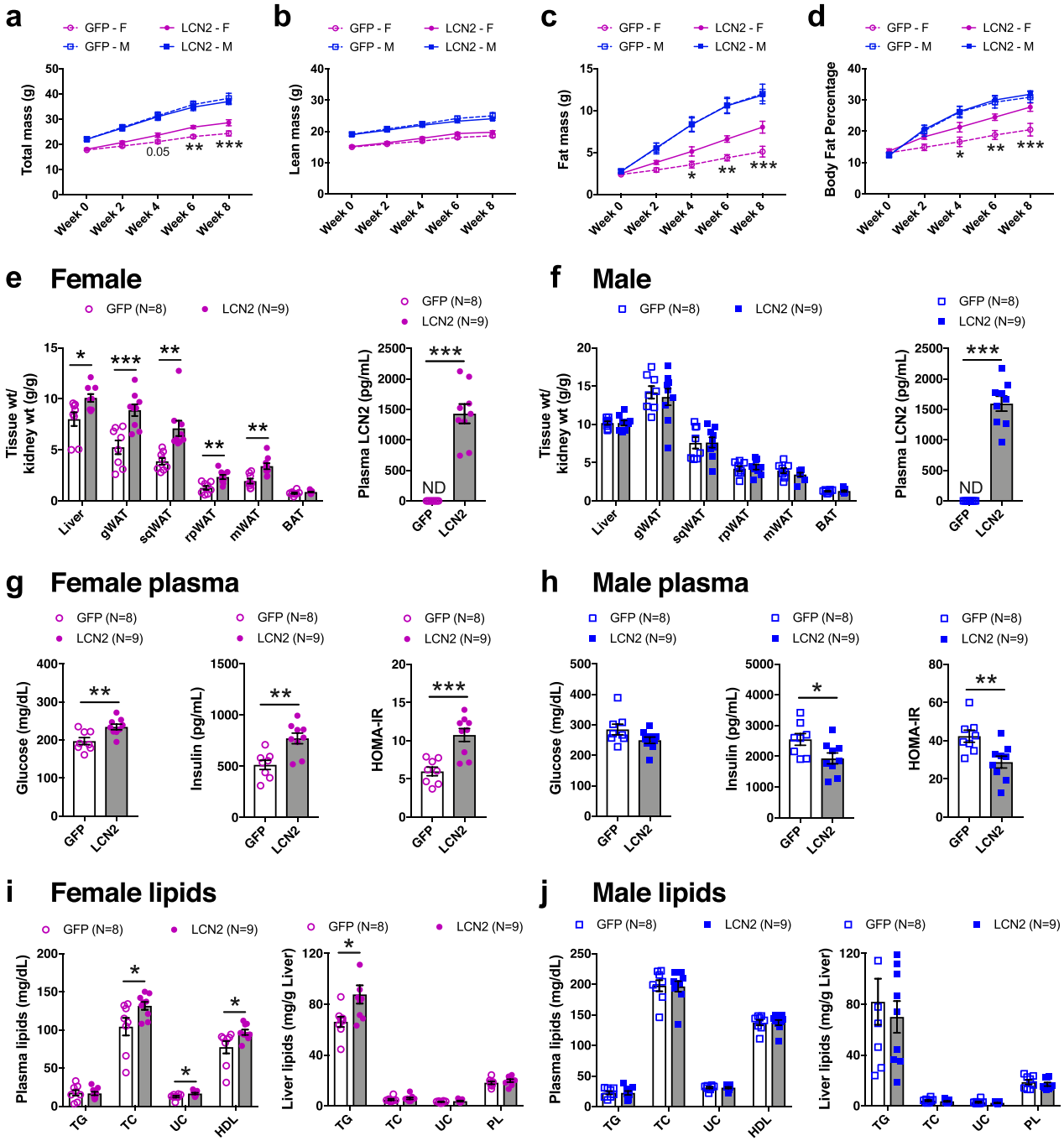

Figure 2: Females overexpressing adipose LCN2 exhibit obesity and other metabolic complications. Eight-week old females and males of *Lcn2*-null mice were injected with AAV vectors carrying either GFP or LCN2 cDNA under the control of adiponectin promoter and fed with HF/HS diet for eight additional weeks. Body weight composition such as **A,** total mass **B,** lean mass **C,** fat mass, and **D,** body fat percentage were monitored every two weeks. Comparisons of kidney-normalized tissue weights and plasma levels of LCN2 between GFP and LCN2 groups in **E,** females and **F,** males, respectively. Comparisons of plasma levels of glucose, insulin, and HOMA-IR from **G,** female and **H,** male animals, respectively. Similarly, comparisons of plasma levels of triglycerides (TG), total cholesterol (TC), unesterified cholesterol (UC) and HDL as well as hepatic TG, TC, UC and phospholipid (PL) levels from **I,** female and **J,** male animals, respectively. Data are presented as mean ± SEM (n = 8–9 animals). *P* values were calculated by **A** – **D,** Repeated-measures 2-factor ANOVA corrected by post-hoc "Holm-Sidak's" multiple comparisons test; **E** – **J,** Unpaired Student's t test for tissue weights, plasma and liver analytes. $*P < 0.05$; $**P < 0.01$; $***P < 0.001$. See also Figures S4–S7.

outlined in Figure 3A. We extended the time period to 16-weeks in order to allow, for each test, a 2-weeks interval to give sufficient time for the mice to recuperate. Similar to our prior experiments in *Lcn2*-null mice, adipose LCN2 overexpression significantly increased fat mass and total mass in the WT animals after 8-weeks of HF/HS diet (Figure 3B). Interestingly, lean mass was also increased in these animals (Figure 3B). To check if the enhanced lean mass in WT animals was due to differences in the extent of AAV-mediated *Lcn2* expression

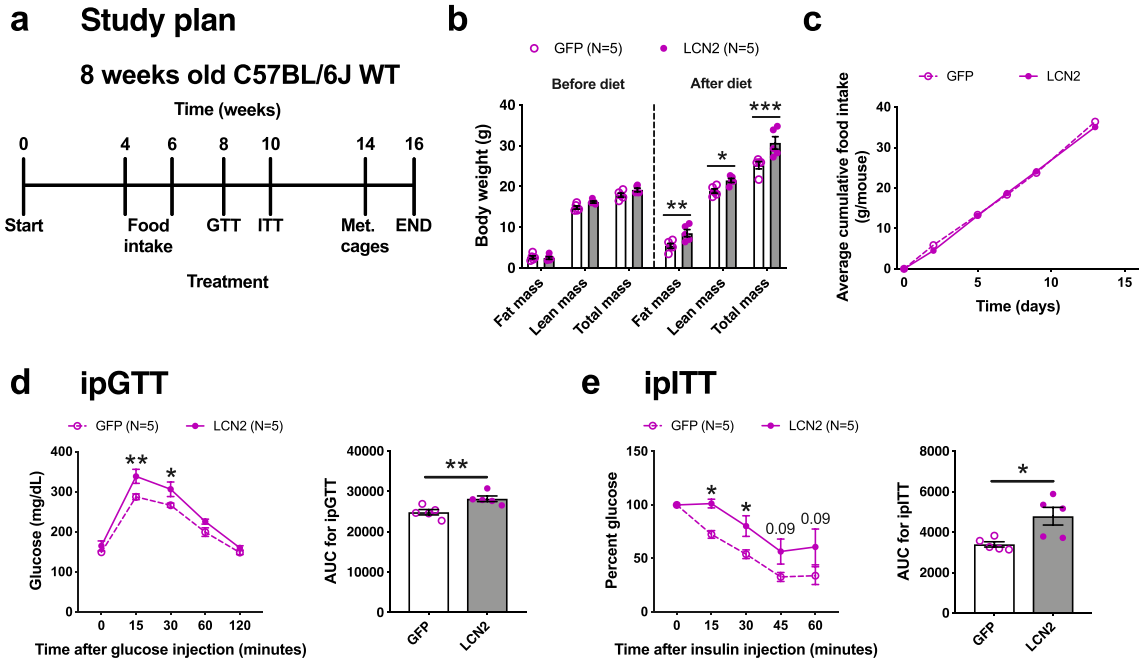

Figure 3: Effects of long term adipose LCN2 overexpression. A, Study plan for long-term adipose LCN2 overexpression in female C57BL/6J wildtype (WT). **B,** Fat mass, lean mass, and total mass before and after 8-weeks of HF/HS diet challenge. **C,** Cumulative food consumption between GFP and LCN2 groups. **D,** Glucose-tolerance test and **E,** Insulin-tolerance test and their respective AUC of adipose-specific GFP or LCN2 overexpressing females after 8- and 10- weeks of diet challenge. Data are presented as mean ± SEM (n = 5 animals per group). *P* values were calculated by **B,** 3-factor ANOVA corrected by post-hoc "Holm-Sidak's" multiple comparisons test; **D and E,** Repeated measures 2-factor ANOVA corrected by post-hoc "Holm-Sidak's" multiple comparisons test; **D and E,** Unpaired Student's t test for AUC. $*P < 0.05$; $**P < 0.01$; $***P < 0.001$.

between WT and KO mice, we quantified *Lcn2* expression in multiple adipose depots isolated from both animals. However, the extent of LCN2 overexpression was different in a depot-specific manner between WT and KO mice (Supplemental Figure S4). The gWAT of WT mice had lower while the sqWAT and BAT had higher expression levels compared to KO mice. The sqWAT of WT mice had very high expression levels that the AAV couldn't increase it anymore. Based on this, we could not come to any conclusions as to why there was an enhanced lean mass in WT mice. A recent study has reported that bone-derived LCN2 can control appetite in males [11]. Therefore, we measured food consumption between the two groups over two weeks (weeks 4–6 of diet) but observed no significant changes between the groups (Figure 3C). Consistent with our LCN2 rescue studies in *Lcn2*-null mice, LCN2 overexpressing WT females were glucose intolerant (Figure 3D) and insulin resistant (Figure 3E).

3.6. Adipose LCN2 reduces energy expenditure and promotes systemic insulin resistance through white adipose tissue mitochondrial dysfunction

To understand the effects of adipose LCN2 overexpression on energy homeostasis, animals were individually housed in metabolic chambers for three days (acclimation) after which metabolic measurements were made for two days (Figure 3A). Although the food consumption was similar between the two groups (Supplemental Figure S10a), oxygen consumption rate (VO_2), carbon dioxide production rate (VCO_2) and energy expenditure (EE), normalized to whole body weight, were reduced in LCN2 overexpressing animals compared to controls (Figure 4A–C). Detailed traces are shown in Supplemental Figure S10b–e. When we normalized these measurements (VO_2, VCO_2, and EE) to the corresponding lean body mass, we observed a reduction as well, but it was not statistically significant (Supplemental Figure S11a–f). In this regard, when we plotted unnormalized EE vs. lean body mass, we observed a large reduction in the slope value of the regression of EE capacity vs. lean mass in LCN2 animals (Supplemental Figure S11g). Altogether, these results support the concept that defects in EE induced by LCN2 overexpression contribute to fat accumulation in adipose tissue. Remarkably, LCN2 overexpressing mice showed lower RER values (Figure 4D), a symptom of systemic insulin resistance associated with reduced ability to utilize glucose as an oxidative substrate in fed state. Thus, the metabolic cage results support the conclusion that adipose LCN2 overexpression promotes insulin resistance in females.

As mitochondrial function is key to adipose tissue dysfunction, promoting systemic lipotoxicity, insulin resistance, and reduced EE, first we measured mitochondrial DNA content in our 8-week HF/HS diet fed cohort of *Lcn2*-null mice overexpressing adipose LCN2 and observed a marked reduction in females but not males (Figure 4E). To test the functional relevance of this decline in mitochondrial DNA levels, we performed bioenergetic analyses on isolated mitochondria from gonadal adipose tissues of two independent 16-week HF/HS diet fed cohorts of WT (Figure 4F) and *Lcn2*-null mice overexpressing adipose LCN2 (Figure 4G). We observed that the activity of all electron transport chain complexes was reduced in mitochondria isolated from the LCN2 overexpressing animals in both of these independent cohorts (Figures 4F,G). Finally, western blot analysis revealed that LCN2 overexpressing animals have significantly lower levels of complex I, II, and IV proteins compared to their respective controls in both of these cohorts (Figure 4H–J).

To directly determine if LCN2 might be causal in mediating mitochondrial dysfunction in adipose, we performed bioenergetic analyses on *ex vivo* differentiated periovarian adipocytes, isolated from female *Lcn2*-null mice, treated with recombinant LCN2 protein. We observed a

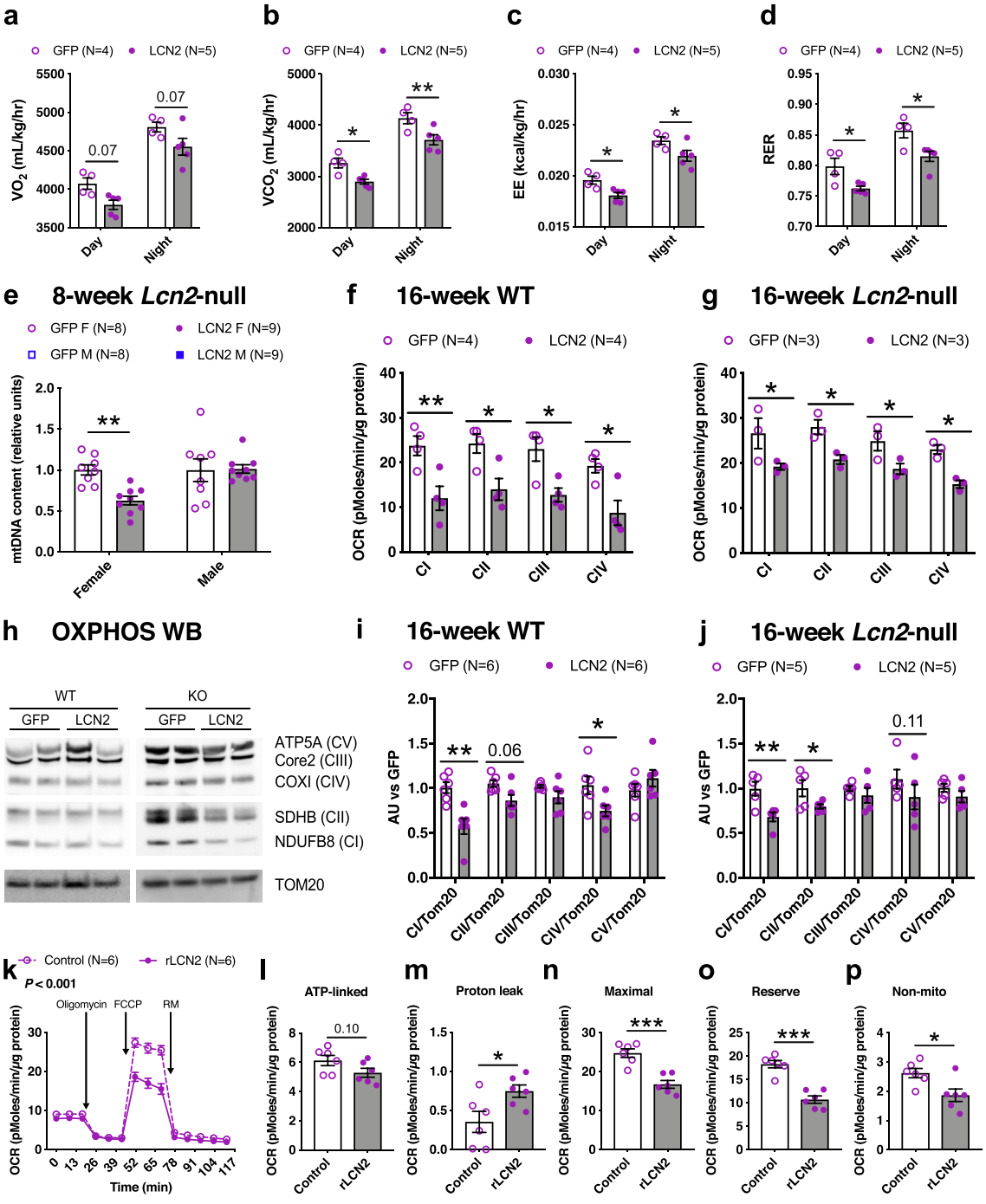

Figure 4: Adipose LCN2 reduced energy expenditure, mitochondrial respiration, mitochondrial DNA content, mitochondrial complex activity, and protein levels. After 14-weeks of HF/HS diet challenge, animals were individually housed in metabolic cages to measure **A,** oxygen consumption rate (VO_2), **B,** carbon dioxide production rate (VCO_2), **C,** energy expenditure (EE) and **D,** respiratory exchange rate (RER) between GFP and LCN2 overexpressing females. To examine mitochondrial dysfunction **E,** relative mitochondrial DNA content in gonadal adipose of females and males overexpressing GFP or LCN2 were measured. Electron flow assays of isolated gonadal adipose mitochondria from **F,** WT and **G,** *Lcn2*-null females overexpressing GFP or LCN2 after 16-weeks of HF/HS diet challenge. **H,** Representative western blot probed with antibodies of OXPHOS complex subunits I—V (CI—CV) and TOM20 as a loading control, and corresponding quantifications from **I,** WT and **J,** *Lcn2*-null females overexpressing GFP or LCN2. Comparisons between control and recombinant LCN2-treated groups of *ex vivo* differentiated periovarian adipocytes in **K,** oxygen consumption rate (OCR) profile, **L,** ATP-linked (datapoint 6 subtracted from 3), **M,** proton leak (datapoint 14 subtracted from 6), **N,** maximal respiratory capacity (datapoint 14 subtracted from 7), **O,** reserve capacity (datapoint 3 subtracted from 7), and **P,** non-mitochondrial (datapoint 14) associated respiration levels. Data are presented as mean ± SEM (n = 4—5 animals per group for **A** — **D**; n = 8—9 animals per group for **E**; n = 3—6 mitochondria per group for **F** — **J**; n = 6 per group for **K** — **P**). *P* values were calculated by **A** — **D,** Repeated measures 2-factor ANOVA corrected by post-hoc "Holm-Sidak's" multiple comparisons test; **E** — **G,** 2-factor ANOVA corrected by post-hoc "Holm-Sidak's" multiple comparisons test; **I and J,** Multiple Student's t tests corrected by "Benjamini, Krieger, Yekutieli" FDR approach for multiple comparisons test; **K,** Repeated measures 2-factor ANOVA; **L** — **P,** Unpaired Student's t test. $*P < 0.05$; $**P < 0.01$; $***P < 0.001$. See also Figures S10—S12.

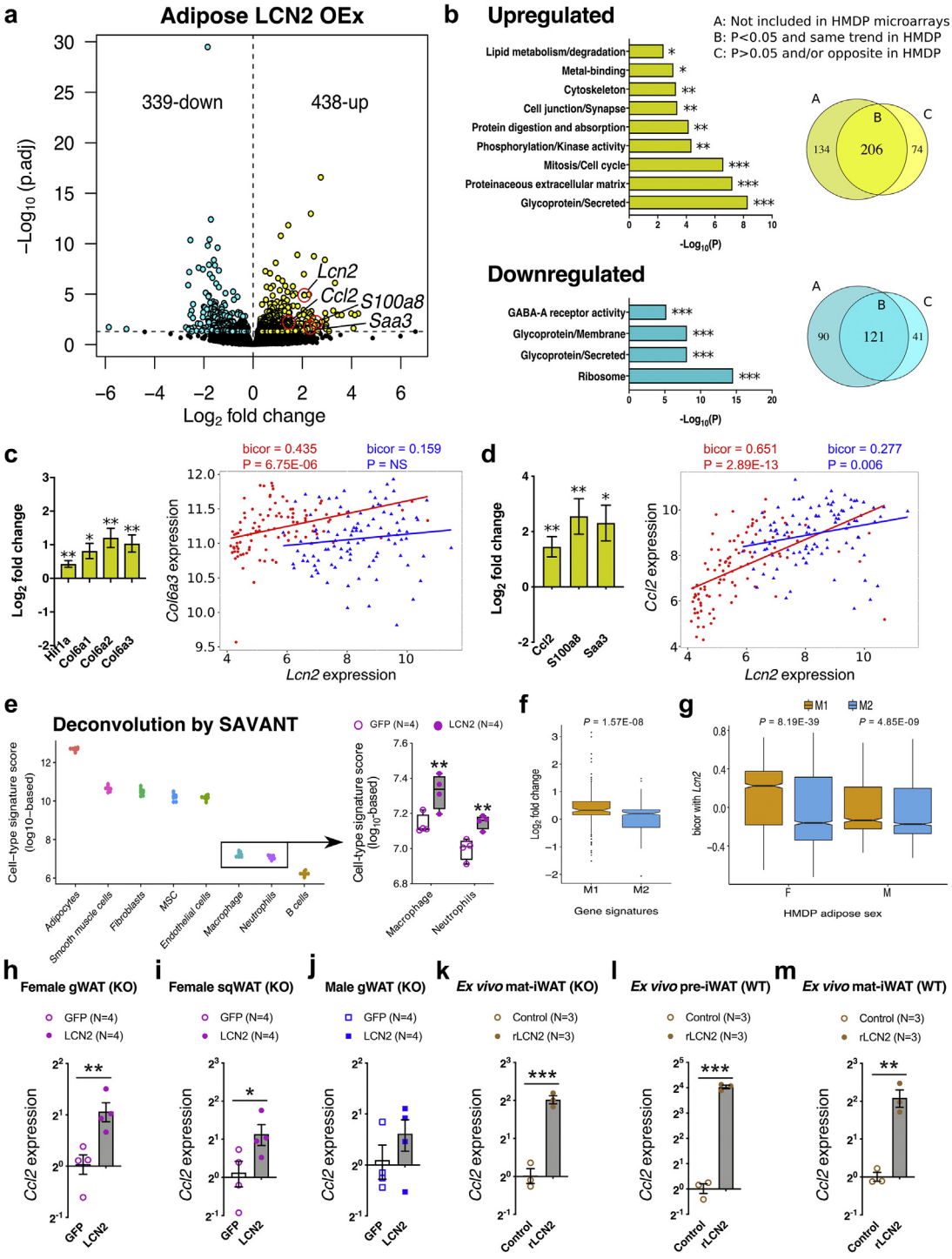

Figure 5: Adipose LCN2 overexpression increases inflammation and fibrosis gene signatures in females. A, Global genome-wide transcriptomics revealed 777 differentially expressed transcripts (5% FDR cutoff) between GFP and LCN2 overexpressing adipose tissues extracted from *Lcn2*-null females fed a HF/HS diet for 8-weeks. **B,** Pathway/process enrichment analyses of upregulated and downregulated transcripts and Comparisons between differentially expressed transcripts and HMDP transcript associations. Log_2 fold change expression values of **C,** fibrosis-associated transcripts such as *Hif1a*, *Col6a1*, *Col6a2*, and *Col6a3*; and **D,** inflammation-associated transcripts such as *Ccl2*, *S100a8*, and *Saa3* between GFP and LCN2 overexpressing female adipose and their respective bicorrelations with adipose *Lcn2* expression in female (red) and male (blue) HMDP cohorts (n = 98 sex-matched strains). **E,** Adipose deconvolution with a specific focus on inflammatory cell populations. **F,** Log_2 fold change expression values of M1 or M2 macrophage-associated gene transcripts between the two groups and **G,** their respective bicorrelations with adipose *Lcn2* expression in female and male HMDP cohorts. Relative normalized expression values of *Ccl2* in **H,** female gonadal WAT **I,** female subcutaneous WAT and **J,** male gonadal WAT overexpressing GFP and LCN2, **K**–**M,** *ex vivo* pre- or differentiated primary inguinal adipocytes isolated from *Lcn2*-null or C57BL/6J wildtype mice treated with recombinant LCN2 overexpressing GFP and LCN2. Data are presented as mean ± SEM (n = 4 mouse/group for global RNA sequencing; n = 4 mouse/group for qPCR; n = 6 female mouse/iWAT divided into two groups for *ex vivo* treatment). *P* values (and *Q* values for RNA sequencing data) were calculated by DESeq function of Bioconductor R-package for RNA sequencing; BicorAndPvalue function of the WGCNA R-package for HMDP transcript associations; Unpaired Student's t test for qPCR. **P* or *Q* < 0.05; ***P* or *Q* < 0.01; ****P* or *Q* < 0.001. See also Figure S13 and Table S2.

significantly reduced respiration profile in LCN2-treated cells (Figure 4K), confirming our observations that LCN2 is causal in mediating mitochondrial dysfunction as seen *in vivo* in Figure 4E—J. We also observed a reduced respiration profile in *ex vivo* differentiated inguinal adipocytes (iWAT), isolated from female WT mice, treated with recombinant LCN2 protein (Supplementary Figure S12a). Similarly, a reduced respiration profile was observed in *ex vivo* differentiated WT iWAT compared to KO iWAT without any exogenous recombinant LCN2 treatment (Supplementary Figure S12b). Furthermore, individual measurements revealed that ATP-linked respiration, maximal respiratory capacity, reserve capacity, and non-mitochondrial respiration decreased while proton leak increased in response to recombinant LCN2 treatment (Figure 4L—P). Taken together, we conclude that LCN2 associated metabolic complications are mediated, at least in part, through mitochondrial dysfunction in adipose tissue.

3.7. Increased adipose LCN2 promotes a gene expression signature of inflammation and fibrosis in adipose tissue from females but not males

To further explore the mechanistic role of adipose LCN2 in metabolic traits, we performed whole-genome transcriptomics on gonadal fat tissues of female *Lcn2*-null mice overexpressing either GFP or LCN2 in their adipose tissues and fed a HF/HS diet for 8-weeks. We found 777 differentially expressed transcripts (5% FDR cutoff) between the two treatments (Figure 5A and Supplemental Table S2). Enrichment analysis, DAVID [69], ToppGene [70], revealed downregulation of pathways associated with ribosome assembly, N-linked glycosylation and GABA-A receptor activity and upregulation of gene pathways associated with collagen metabolism, proteinaceous extracellular matrix and cell cycle/mitosis (Figure 5B). The relationships between LCN2 expression and transcript levels of other genes in adipose that we observed in the HMDP study were largely consistent with the results of the tissue-specific expression studies. Thus, of the 280/414 upregulated transcripts observed in the HMDP studies, 73.5% (206 transcripts) changed in the same direction in LCN2 overexpressing females (positively correlated in HMDP and upregulated in LCN2 overexpressing females). On the other hand, among the 162/252 downregulated transcripts observed in the HMDP studies, 74.7% (121 transcripts) went in the same direction (Figure 5B).

We observed that overexpression of LCN2 in female adipose was associated with markers of both fibrosis and inflammation. These included the adipose fibrosis markers, hypoxia-inducible factor 1 alpha (HIF1A) [71,72] and collagen VI subunit (COL6A3) [73,74] and the adipose inflammation markers, monocyte chemoattractant protein-1 (MCP1/CCL2) [75], S100A8 [76] and SAA3 [77] (Figure 5A,C,D). Similar associations between LCN2 and the fibrosis/inflammation genes were observed across the HMDP strains in females but not males (Figure 5C,D).

Beyond these representative marker genes, we investigated whether there were any global differences in inflammatory cell composition between the two groups. To this end, we performed deconvolution analyses using an existing deconvolution algorithm (SaVanT, http://newpathways.mcdb.ucla.edu/savant-dev). As shown in Figure 5E, when focused on inflammatory cells, both macrophage and neutrophil populations were significantly higher in LCN2 groups. Differences in other cell populations were shown in Fig. S13a. To further investigate what subtypes of macrophages (M1 vs. M2) were enriched in these LCN2 groups, we used macrophage gene signatures identified previously using our diverse HMDP populations [78]. We observed M1 gene signatures were selectively upregulated in our LCN2 groups (Figure 5F). Moreover, our HMDP populations also revealed that female strains had significantly higher M1 gene signatures correlated with *Lcn2* expression compared to their male counterparts (Figure 5G). Follow-up quantitative PCR measurements on gonadal and subcutaneous adipose tissues extracted from GFP or LCN2 overexpressing mice confirmed these observations (Figure 5H—J).

To directly determine if LCN2 was causal in mediating these transcriptional changes, we treated *ex vivo* pre- or mature/differentiated inguinal adipocytes isolated from female *Lcn2*-null or WT mice with recombinant LCN2 protein and observed increased *Ccl2* expression, confirming our observations (Figure 5K—M). However, no other inflammatory marker genes were significantly different in gWAT isolated from LCN2 overexpressing mice (Supplementary Figure S13b). Indeed, a similar increase only in CCL2 was observed when estradiol/ERα inhibition of LCN2 was removed [35]. Taken together, our data support the concept that adipose-derived LCN2 mediated inflammation and fibrosis contributes to the metabolic complications accompanying diet-induced obesity.

3.8. Adipose LCN2 negatively regulate its receptor LRP2 and repressor ERα in a female-specific manner

We further explored our transcriptomics data to identify molecular mediators of LCN2 action. We first examined the expression data for LCN2 receptors since LCN2 is a secreted protein. So far, two receptors have been characterized to bind LCN2 and mediate its uptake *via* receptor-mediated endocytosis: SLC22A17 [79] and LDL receptor-related protein 2 (LRP2) or megalin [80]. Of these, we found that *Lrp2* was downregulated in LCN2 overexpressing females (Figure 6A). Next, we investigated a female-specific repressor of LCN2, estrogen receptor alpha (ERα). To our surprise, we observed a reduction in *Esr1* expression in LCN2 overexpressing females (Figure 6A). Consistent with this, when we inspected the HMDP for transcript associations, we observed that adipose *Lcn2* showed sex-specific correlations to both these transcripts between sexes: *Lrp2* showed a negative correlation in females and a positive correlation in males, while *Esr1* showed a negative correlation in females and no correlation in males (Figure 6B). Follow-up quantitative PCR measurements on female and male gonadal adipose tissues extracted from GFP or LCN2 overexpressing mice confirmed these observations (Figure 6C,D). Similar observations were seen in female subcutaneous and brown adipose tissues as well (Figure 6E,F). Moreover, we also observed reduced ERα and LRP2 protein levels with LCN2 overexpression *via* western blot analyses (Supplementary Figure S14a). Also, primary mature adipocytes isolated from both sexes of WT mice revealed that female adipocytes had higher basal *Lrp2* expression levels than males (Supplementary Figure S14b). Further experiments on primary adipocytes isolated from *Lcn2*-null mice treated with recombinant LCN2 protein to determine the causality of LCN2 in mediating the downregulation of *Lrp2* and *Esr1* confirmed our observations (Figure 6G,H). Similarly, we observed that primary adipocytes from WT females had reduced levels of both *Lcn2* and *Esr1* expression levels as compared to KO mice (Supplementary Figure S14c). Furthermore, when we treated primary, pre- or mature adipocytes isolated from WT mice with recombinant LCN2 protein, besides reduction in both LRP2 and ERα expression, we observed an increase in endogenous *Lcn2* expression (Figure 6I,J). This was indeed a surprise to us, because it has been previously demonstrated that ERα inhibits adipose LCN2 expression [35]. This feedback inhibition of ERα by rLCN2 and a subsequent increase in *Lcn2* expression is a novel observation.

When we interrogated the HMDP populations to check for association(s) between adipose *Lrp2* expression and metabolic traits, we observed that in females but not in males, adipose *Lrp2* expression

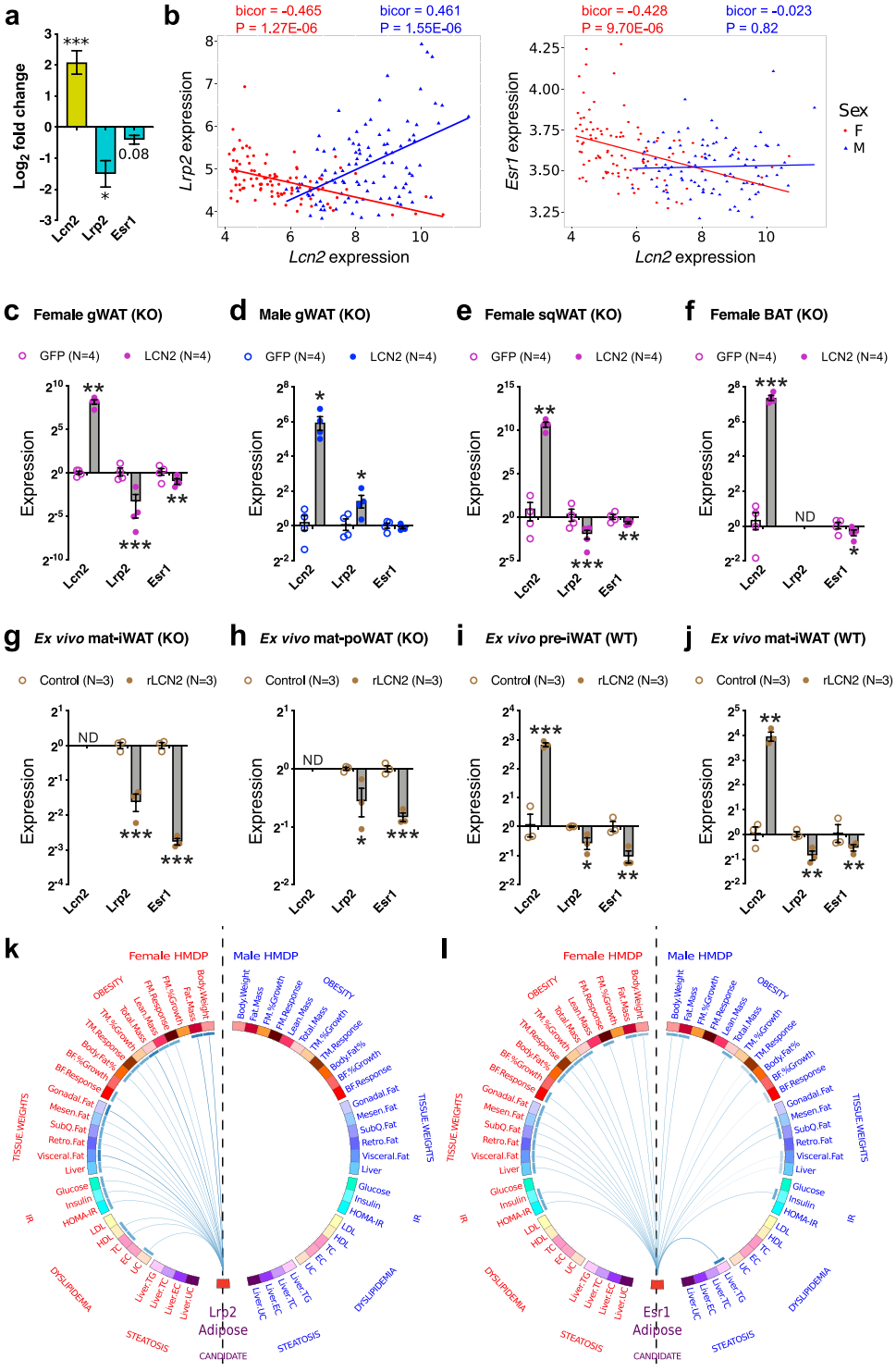

Figure 6: Adipose LCN2 downregulates expression of both LRP2 and ERα. Log_2 fold change expression values of **A,** *Lcn2*, *Lrp2*, and *Esr1* between GFP and LCN2 overexpressing female adipose and **B,** their respective bicorrelations with adipose *Lcn2* expression in female and male HMDP cohorts (n = 98 sex-matched strains). Relative normalized expression values of *Lcn2*, *Lrp2*, and *Esr1* in **C,** female gonadal WAT **D,** male gonadal WAT **E,** female subcutaneous WAT and **F,** female BAT overexpressing GFP and LCN2, **G – J,** *ex vivo* pre- or differentiated primary inguinal or periovarian adipocytes isolated from female *Lcn2*-null or C57BL/6J wildtype mice treated with recombinant LCN2. Circos connectogram plot showing biweight midcorrelation between adipose **K,** *Lrp2* or **L,** *Esr1* expression and metabolic traits in female and male HMDP cohort (n = 102 female and 111 male strains). Each connecting line signify a significant (1% FDR cutoff) bicorrelation between *Lrp2* or *Esr1* expression and the respective trait. Blue line indicates negative correlation and the color intensity signify the magnitude of correlation. Data are presented as mean ± SEM (n = 4 mouse/group for global RNA sequencing; n = 4 mouse/group for qPCR; n = 6 female mouse/iWAT divided into two groups for *ex vivo* treatment). *P* values (and *Q* values for RNA sequencing data) were calculated by DESeq function of Bioconductor R-package for RNA sequencing; BicorAndPvalue function of the WGCNA R-package for HMDP transcript associations; Unpaired Student's t test for qPCR. **P* or *Q* < 0.05; ***P* or *Q* < 0.01; ****P* or *Q* < 0.001. See also Figures S1,S14–15 and Table S1.

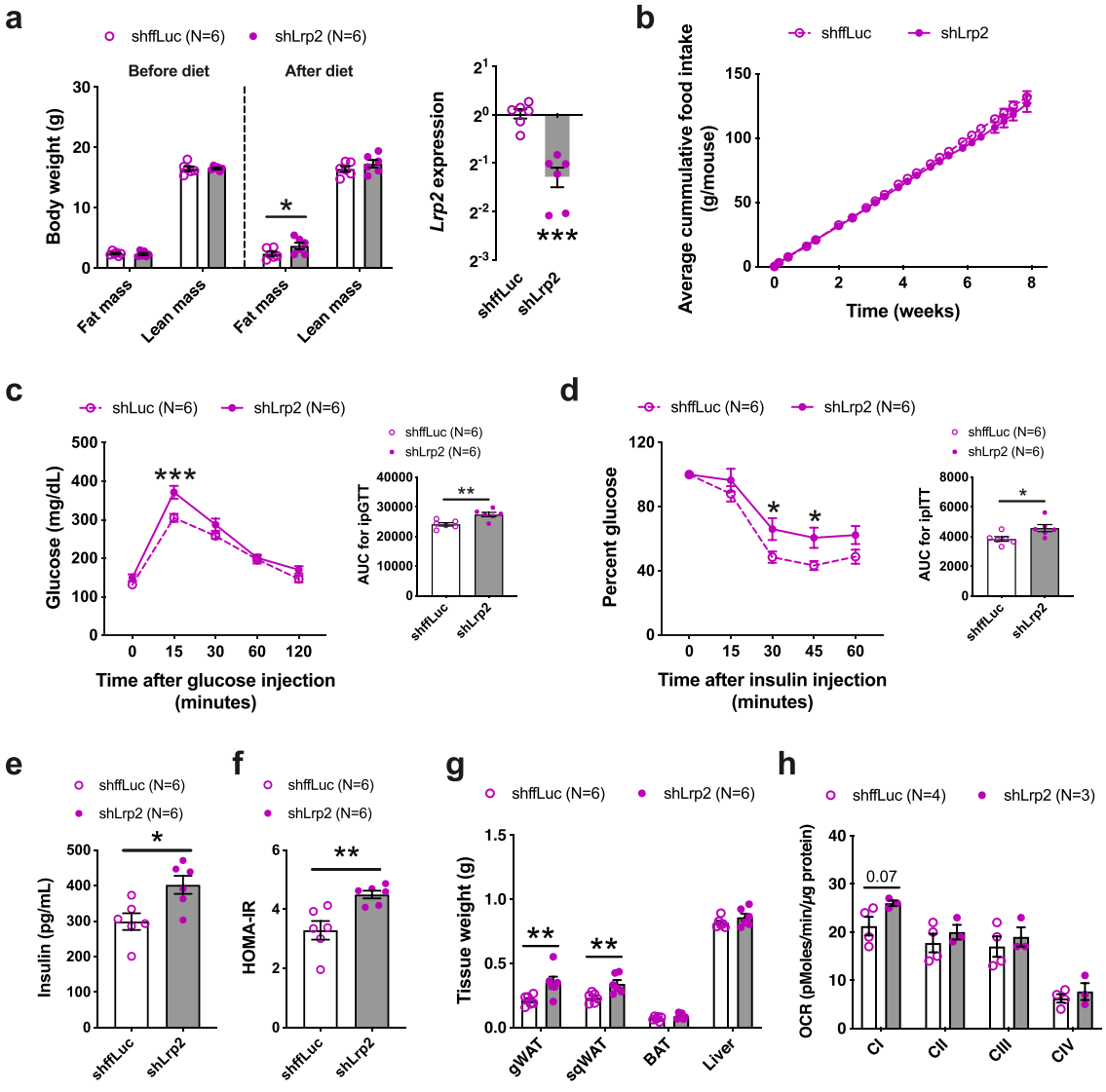

Figure 7: Females with adipose LRP2 knockdown exhibit obesity and other metabolic disturbances. A, Fat mass and lean mass before and after 8-weeks of HF/HS diet challenge along with *Lrp2* expression between the two groups. **B,** Cumulative food consumption between control and shLrp2 groups. **C,** Glucose-tolerance test and **D,** Insulin-tolerance test and their respective AUC of adipose-specific control or shLrp2 females after 8- and 10- weeks of diet challenge. Comparisons of **E,** plasma levels of insulin **F,** HOMA-IR and **G,** tissue weights and **H,** Electron flow assays of isolated gonadal adipose mitochondria between the two groups after HF/HS diet challenge. Data are presented as mean ± SEM (n = 6 animals per group for **A** − **G**; n = 3–4 mitochondria per group for **H**). *P* values were calculated by **A,** 3-factor ANOVA corrected by post-hoc "Holm-Sidak's" multiple comparisons test; **A,** Unpaired Student's t test for gene expression**; C and D,** Repeated measures 2-factor ANOVA corrected by post-hoc "Holm-Sidak's" multiple comparisons test; **C** − **F,** Unpaired Student's t test for AUC and insulin panel; **G and H,** 2-factor ANOVA corrected by post-hoc "Holm-Sidak's" multiple comparisons test. $^{*}P < 0.05$; $^{**}P < 0.01$; $^{***}P < 0.001$.

was strongly and negatively (1% FDR cutoff) associated with obesity, tissue weights, dyslipidemia, and insulin resistance (Figure 6K). In contrast, we observed that adipose *Esr1* expression was strongly and negatively (1% FDR cutoff) associated with metabolic traits in both sexes (Figure 6L). These two gene—trait associations were in the opposite direction of what we observed for adipose *Lcn2* in Figure 1G. Individual bicorrelation coefficients and *P* values for each association are listed in Supplemental Table S1. Taken together, our data suggest that the female-specific adipose LCN2 action is mediated, at least in part, through negative regulation of its receptor, LRP2, and its repressor, ERα.

3.9. Adipose LRP2 inhibition alters obesity and insulin resistance in females

As a proof of concept, we used our AAV system to knockdown *Lrp2* expression in adipose tissues of C57BL/6J WT mice followed by feeding a HF/HS diet. We observed a minor increase in fat mass on sh*Lrp2* mice (Figure 7A) with no change in food intake between the two groups (Figure 7B). We also observed increased glucose intolerance and insulin resistance in shLrp2 mice as seen through GTT, ITT, fasting insulin, and HOMA-IR levels (Figure 7C—F). End-point organ weights demonstrated that only WAT depots were increased, and no changes were seen in BAT and liver weights (Figure 7G). We also observed a

trend toward an increase in the activity of adipose mitochondrial complex I (Figure 7H). Taken together, these results demonstrate that female-specific adipose LCN2 functions are partly mediated through adipose *Lrp2* expression.

4. DISCUSSION

We have identified a novel sex-specific role for adipose-secreted LCN2 in regulating diet-induced metabolic complications such as obesity, dyslipidemia, insulin resistance and fatty liver. Thus, in adipose, LCN2 exerts sex-specific control of mitochondrial content and activity and promotes tissue remodeling and inflammation, acting in an autocrine/paracrine manner, and this in turn mediates the sex dimorphic metabolic complications. In contrast, the expression of LCN2 in liver showed no significant effects on metabolic functions despite the fact that circulating LCN2 levels increased. Unlike previous studies utilizing a single mouse strain (male *Lcn2*-null or WT C57BL/6J) to implicate LCN2 in metabolic dysfunction, our study used an extensively phenotyped mouse cohort of ~100 classical inbred and recombinant inbred strains of both sexes to identify sex-specific associations. To validate the resulting hypotheses, we used a tissue-specific LCN2 overexpression system *via* AAV-mediated gene transfer. To exclude LCN2 from any source other than our intended tissue, we used a *Lcn2*-null background for our tissue-specific overexpression. As several other studies have produced conflicting results possibly due to the differences in generating *Lcn2*-null mice, we repeated our overexpression studies in a C57BL/6J WT background to exclude any such bias.

It is noteworthy that the results of our experimental LCN2 overexpression studies are entirely consistent with the natural variation in LCN2 expression observed in the HMDP population, such as metabolic effects and gene expression differences. Thus, they do not appear to be due to artifactual effects of overexpression. Our genetic analyses in the HMDP also support the possibility that *Lcn2* expression is regulated in trans by *Lipin1* variation, although further studies are required to confirm this. Nevertheless, our analyses also have some technical limitations. For instance, overexpression of adipose LCN2 in males improved glucose metabolism without affecting body weight but we were not able to predict this through HMDP correlations. We suspect that this may be a statistical issue. The HMDP is a panel of ~100 inbred strains of mice. Correlation analyses using such a population often involve correction by multiple testing. In order to observe a significant correlation between two traits, the effect size must be large enough that it passes the multiple correction tests. On other hand, our study also lacks any thermogenesis-related traits such as BAT transcriptomics, BAT mitochondria, or rectal temperature following cold exposure to detect any male-specific thermogenesis-related correlations as observed by others [81]. Because our primary focus was to understand LCN2-mediated female-specific metabolic complications, we did limited follow-up on other metabolic traits possibly altered in the male overexpressing LCN2.

Although LCN2 has been implicated in metabolic dysfunction, most previous studies examined only one sex, and, in the majority of these studies, whole-body knockout mice and/or circulating LCN2 levels were utilized. For instance, previous studies have reported neutrophil-secreted LCN2 as a key player in regulating alcoholic (female *Lcn2*-null mice with adoptive transfer of WT neutrophils) and non-alcoholic steatohepatitis (male *Lcn2*-null mice with chronic infusion of recombinant LCN2) *via* neutrophil infiltration [18,19]. Another study utilizing bone-specific knockout mouse models demonstrated that bone-secreted LCN2 controls appetite in male mice [11]. More relevant to this paper, a very recent study utilizing adipose-specific LCN2 overexpression in aged male mice (10-months and 18-months old) observed protection against age-related metabolic traits such as glucose intolerance and hepatic steatosis partly through improving adaptive thermogenesis [82]. Here, we demonstrate that 8-week LCN2 overexpressing *Lcn2*-null males also had improved glucose tolerance but no changes otherwise. In complete contrast, we report that adipose-secreted LCN2 regulates obesity in female mice, in both *Lcn2*-null and WT strains, through effects on adipose inflammation, remodeling and mitochondrial dysfunction without changing food consumption. Most of the human associations were made using circulating LCN2 levels due to the inherent difficulty in acquiring other clinical tissues and our studies emphasize the importance of the sex and tissue source of LCN2.

Mitochondrial dysfunction in WAT is associated with obesity and whole body insulin resistance in both animal and human studies [83–88]. In this study, we demonstrate that adipose-derived LCN2 affects mitochondria in female adipose tissues. Notably, LCN2 overexpression lowers the mitochondrial DNA content, electron transport complexes, and the functional capacity per mitochondrion in female adipose tissues. Indeed, LCN2 has been associated with mitochondrial dysfunction in both liver [89,90] and cardiomyocytes [91–93]. Given that estrogens, through ERα, control mitochondrial biogenesis and function [94], and our data demonstrating that LCN2 downregulates ERα, we propose that LCN2-mediated mitochondrial dysfunction could be a result of ERα inhibition. Indeed, Ribas et al., have demonstrated that *Polg1* expression is under the control of ERα in skeletal muscle using ERα antagonist ICI 182,780 (fulvestrant) or an ERα DNA binding mutation (ERα DBDΔ) [95]. More specific to this paper, ERα KO in 3T3-L1 and adipose tissues of mice downregulate *Polg1* (mtDNA polymerase) expression and controls mitochondrial biogenesis (unpublished data, manuscript under review). Furthermore, we observed *Polg1* downregulation concurrently with *Esr1* downregulation in female adipose tissue overexpressing LCN2 or primary adipocytes treated with rLCN2 or primary adipocytes from WT mice. This illustrates a mechanistic role for LCN2 in mediating mitochondrial dysfunction through the ERα-POLG1 axis (Supplementary Figure S15).

Both inflammation and fibrosis of adipose are widely recognized as causal in the development of metabolic dysfunctions such as insulin resistance [71–75,96]. While investigating the mechanistic basis for LCN2 contribution to sex-specific diet-induced obesity, we found that LCN2 induces both pro-inflammatory- and fibrosis-related transcripts including *Ccl2*, *Hif1a*, and *Col6a3* expression in female adipose tissues. Using our mouse population, we also show that these transcripts are not associated with adipose LCN2 expression in male adipose tissues. Further analyses establish that *Lrp2*, a cell-surface LCN2 receptor, is negatively regulated in females. LRP2 or megalin is a 600 kDa member of low-density lipoprotein receptor family and is an endocytic receptor that binds LCN2 with high affinity [80]. Besides LCN2, megalin transports numerous ligands including vitamin A, B12, and D, along with their transport proteins, leptin, angiotensin II, insulin, and albumin [97]. Notably, LRP2 also binds and endocytoses sex hormone binding globulin that mediates uptake of both androgens and estrogens [98]. Though megalin is primarily expressed in epithelial cells, megalin expression has been observed in 3T3-L1 adipocytes, human primary adipocytes, and mouse gWAT in response to vitamin D [99,100] and in 3T3-L1 adipocytes in response to angiotensin II [101]. Our studies also revealed striking negative associations between metabolic traits and adipose LRP2 expression (Figure 6K). Our LRP2 inhibition studies in female adipose tissues validated some of these associations and support the conclusion that LCN2 action is mediated

in part through negative regulation of LRP2. Further investigations are required to identify how LCN2 regulates *Lrp2* transcription in a sex-specific manner.

One of our most interesting and unexpected findings was that LCN2 can downregulate ERα in female adipose, both *in vitro* and *in vivo*. Given that adipose *Lcn2* expression is directly inhibited by ERα binding [35] and is positively associated with metabolic traits only in females (Figure 1G), it is likely that the observed female-specific negative regulation of ERα by LCN2 is part of an intricate feedback mechanism. Adipose-specific ERα KO increases obesity in mice of both sexes [35]. Indeed, our HMDP populations revealed striking negative associations between metabolic traits and ERα expression in both sexes. Intriguingly, only female ERα expression was inhibited by LCN2 in our studies, partly explaining the pathological role of LCN2 in females. Future studies are warranted to delineate how LCN2 inhibits *Esr1* transcription in female adipose tissues.

In summary, our studies make it clear that LCN2 exhibits diverse and at times antagonistic context-, tissue- and sex-dependent roles. Any pharmacological targeting of LCN2 as a treatment for metabolic dysfunction will have to account for these. Importantly, our study exemplifies the need to include both sexes while studying complex traits to optimize genetic contributions and therapeutic intervention.

FUNDING INFORMATION

This work was supported by NIH-PO1HL028481 (A.J.L.), AHA fellowship 18POST33990256 (K.C.K.), NIH-P30DK063491 (M.L.), the Foundation Leducq 12CVD04 (L.V. and K.R.), NIH-K99HL138193 (M.M.S.), and NIH-T32HL69766 (B.K.F.). The funders had no role in study design, data collection and interpretation, or the decision to submit the work for publication.

AUTHOR CONTRIBUTIONS

K.C.K., and A.J.L. conceived the study. K.C.K., S.S., M.S., Y.M., R.A.P., J.M.L., R.F., L.V., M.M.S., B.K.F., D.J., S.N., D.A., C.P., L.S., M.P., K.R., M.L., and A.J.L. performed experiments or analyzed the data. K.C.K., and A.J.L. drafted the manuscript, and all authors read or revised the manuscript.

ACKNOWLEDGEMENTS

We thank Sarada Charugundla for plasma and liver metabolite analyses, Zhiqiang Zhou and Hannah Qi and for assistance in animal experiments, and Nam Che for AAV construction.

CONFLICT OF INTEREST

The authors declare no conflict of interests.

APPENDIX A. SUPPLEMENTARY DATA

Supplementary data to this article can be found online at https://doi.org/10.1016/j.molmet.2019.09.009.

REFERENCES

[1] Kjeldsen, L., Johnsen, A.H., Sengelov, H., Borregaard, N., 1993. Isolation and primary structure of NGAL, a novel protein associated with human neutrophil gelatinase. Journal of Biological Chemistry 268:10425—10432.

[2] Triebel, S., Bläser, J., Reinke, H., Tschesche, H., 1992. A 25 kDa α2-microglobulin-related protein is a component of the 125 kDa form of human gelatinase. FEBS Letters 314:386—388.

[3] Goetz, D.H., Holmes, M.A., Borregaard, N., Bluhm, M.E., Raymond, K.N., Strong, R.K., 2002. The neutrophil lipocalin NGAL is a bacteriostatic agent that interferes with siderophore-mediated iron acquisition. Molecular Cell 10: 1033—1043.

[4] Flo, T.H., Smith, K.D., Sato, S., Rodriguez, D.J., Holmes, M.A., Strong, R.K., et al., 2004. Lipocalin 2 mediates an innate immune response to bacterial infection by sequestrating iron. Nature 432:917—921.

[5] Yan, Q.W., Yang, Q., Mody, N., Graham, T.E., Hsu, C.H., Xu, Z., et al., 2007. The adipokine lipocalin 2 is regulated by obesity and promotes insulin resistance. Diabetes 56:2533—2540.

[6] Catalan, V., Gomez-Ambrosi, J., Rodriguez, A., Ramirez, B., Silva, C., Rotellar, F., et al., 2009. Increased adipose tissue expression of lipocalin-2 in obesity is related to inflammation and matrix metalloproteinase-2 and metalloproteinase-9 activities in humans. Journal of Molecular Medicine (Berl) 87:803—813.

[7] Xu, M.J., Feng, D., Wu, H., Wang, H., Chan, Y., Kolls, J., et al., 2015. Liver is the major source of elevated serum lipocalin-2 levels after bacterial infection or partial hepatectomy: a critical role for IL-6/STAT3. Hepatology 61:692—702.

[8] Borkham-Kamphorst, E., van de Leur, E., Zimmermann, H.W., Karlmark, K.R., Tihaa, L., Haas, U., et al., 2013. Protective effects of lipocalin-2 (LCN2) in acute liver injury suggest a novel function in liver homeostasis. Biochimica et Biophysica Acta 1832:660—673.

[9] Cai, L., Rubin, J., Han, W., Venge, P., Xu, S., 2010. The origin of multiple molecular forms in urine of HNL/NGAL. Clinical Journal of the American Society of Nephrology 5:2229—2235.

[10] Nickolas, T.L., Forster, C.S., Sise, M.E., Barasch, N., Sola-Del Valle, D., Viltard, M., et al., 2012. NGAL (Lcn2) monomer is associated with tubulointerstitial damage in chronic kidney disease. Kidney International 82:718—722.

[11] Mosialou, I., Shikhel, S., Liu, J.M., Maurizi, A., Luo, N., He, Z., et al., 2017. MC4R-dependent suppression of appetite by bone-derived lipocalin 2. Nature 543:385—390.

[12] Zhang, J., Wu, Y., Zhang, Y., Leroith, D., Bernlohr, D.A., Chen, X., 2008. The role of lipocalin 2 in the regulation of inflammation in adipocytes and macrophages. Molecular Endocrinology 22:1416—1426.

[13] Wang, Y., Lam, K.S., Kraegen, E.W., Sweeney, G., Zhang, J., Tso, A.W., et al., 2007. Lipocalin-2 is an inflammatory marker closely associated with obesity, insulin resistance, and hyperglycemia in humans. Clinical Chemistry 53:34—41.

[14] Auguet, T., Quintero, Y., Terra, X., Martinez, S., Lucas, A., Pellitero, S., et al., 2011. Upregulation of lipocalin 2 in adipose tissues of severely obese women: positive relationship with proinflammatory cytokines. Obesity (Silver Spring) 19:2295—2300.

[15] Guo, H., Jin, D., Zhang, Y., Wright, W., Bazuine, M., Brockman, D.A., et al., 2010. Lipocalin-2 deficiency impairs thermogenesis and potentiates diet-induced insulin resistance in mice. Diabetes 59:1376—1385.

[16] Jun, L.S., Siddall, C.P., Rosen, E.D., 2011. A minor role for lipocalin 2 in high-fat diet-induced glucose intolerance. American Journal of Physiology-Endocrinology and Metabolism 301:E825—E835.

[17] Law, I.K., Xu, A., Lam, K.S., Berger, T., Mak, T.W., Vanhoutte, P.M., et al., 2010. Lipocalin-2 deficiency attenuates insulin resistance associated with aging and obesity. Diabetes 59:872—882.

[18] Wieser, V., Tymoszuk, P., Adolph, T.E., Grander, C., Grabherr, F., Enrich, B., et al., 2016. Lipocalin 2 drives neutrophilic inflammation in alcoholic liver disease. Journal of Hepatology 64:872—880.

[19] Ye, D., Yang, K., Zang, S., Lin, Z., Chau, H.T., Wang, Y., et al., 2016. Lipocalin-2 mediates non-alcoholic steatohepatitis by promoting neutrophil-

macrophage crosstalk via the induction of CXCR2. Journal of Hepatology 65: 988–997.
[20] Solak, Y., Yilmaz, M.I., Siriopol, D., Saglam, M., Unal, H.U., Yaman, H., et al., 2015. Serum neutrophil gelatinase-associated lipocalin is associated with cardiovascular events in patients with chronic kidney disease. International Urology and Nephrology 47:1993–2001.
[21] Eilenberg, W., Stojkovic, S., Piechota-Polanczyk, A., Kaun, C., Rauscher, S., Groger, M., et al., 2016. Neutrophil gelatinase-associated lipocalin (NGAL) is associated with symptomatic carotid atherosclerosis and drives pro-inflammatory state in vitro. European Journal of Vascular and Endovascular Surgery 51:623–631.
[22] Marques, F.Z., Prestes, P.R., Byars, S.G., Ritchie, S.C., Wurtz, P., Patel, S.K., et al., 2017. Experimental and human evidence for lipocalin-2 (neutrophil gelatinase-associated lipocalin [NGAL]) in the development of cardiac hypertrophy and heart failure. Journal of the American Heart Association 6.
[23] Rashad, N.M., El-Shal, A.S., Etewa, R.L., Wadea, F.M., 2017. Lipocalin-2 expression and serum levels as early predictors of type 2 diabetes mellitus in obese women. IUBMB Life 69:88–97.
[24] la Chesnaye, E., Manuel-Apolinar, L., Anda, N., Revilla-Monsalve, M., Islas-Andrade, S., 2016. Gender differences in lipocalin 2 plasmatic levels are correlated with age and the triglyceride/high-density lipoprotein ratio in healthy individuals. Gaceta Médica de México 152:612–617.
[25] Parks, B.W., Nam, E., Org, E., Kostem, E., Norheim, F., Hui, S.T., et al., 2013. Genetic control of obesity and gut microbiota composition in response to high-fat, high-sucrose diet in mice. Cell Metabolism 17:141–152.
[26] Parks, B.W., Sallam, T., Mehrabian, M., Psychogios, N., Hui, S.T., Norheim, F., et al., 2015. Genetic architecture of insulin resistance in the mouse. Cell Metabolism 21:334–347.
[27] Norheim, F., Bjellaas, T., Hui, S.T., Chella Krishnan, K., Lee, J., Gupta, S., et al., 2018. Genetic, dietary, and sex-specific regulation of hepatic ceramides and the relationship between hepatic ceramides and IR. The Journal of Lipid Research 59:1164–1174.
[28] Org, E., Mehrabian, M., Parks, B.W., Shipkova, P., Liu, X., Drake, T.A., et al., 2016. Sex differences and hormonal effects on gut microbiota composition in mice. Gut Microbes 7:313–322.
[29] Org, E., Parks, B.W., Joo, J.W., Emert, B., Schwartzman, W., Kang, E.Y., et al., 2015. Genetic and environmental control of host-gut microbiota interactions. Genome Research 25:1558–1569.
[30] Hui, S.T., Parks, B.W., Org, E., Norheim, F., Che, N., Pan, C., et al., 2015. The genetic architecture of NAFLD among inbred strains of mice. Elife 4:e05607.
[31] Norheim, F., Hui, S.T., Kulahcioglu, E., Mehrabian, M., Cantor, R.M., Pan, C., et al., 2017. Genetic and hormonal control of hepatic steatosis in female and male mice. The Journal of Lipid Research 58:178–187.
[32] Chella Krishnan, K., Kurt, Z., Barrere-Cain, R., Sabir, S., Das, A., Floyd, R., et al., 2018. Integration of multi-omics data from mouse diversity panel highlights mitochondrial dysfunction in non-alcoholic fatty liver disease. Cell Systems 6:103–115 e7.
[33] Hui, S.T., Kurt, Z., Tuominen, I., Norheim, F., Davis, R.C., Pan, C., et al., 2018. The genetic architecture of diet-induced hepatic fibrosis in mice. Hepatology 68:2182–2196.
[34] Guo, H., Zhang, Y., Brockman, D.A., Hahn, W., Bernlohr, D.A., Chen, X., 2012. Lipocalin 2 deficiency alters estradiol production and estrogen receptor signaling in female mice. Endocrinology 153:1183–1193.
[35] Drew, B.G., Hamidi, H., Zhou, Z., Villanueva, C.J., Krum, S.A., Calkin, A.C., et al., 2015. Estrogen receptor (ER)alpha-regulated lipocalin 2 expression in adipose tissue links obesity with breast cancer progression. Journal of Biological Chemistry 290:5566–5581.
[36] Bennett, B.J., Farber, C.R., Orozco, L., Kang, H.M., Ghazalpour, A., Siemers, N., et al., 2010. A high-resolution association mapping panel for the dissection of complex traits in mice. Genome Research 20:281–290.
[37] Leek, J.T., Johnson, W.E., Parker, H.S., Jaffe, A.E., Storey, J.D., 2012. The sva package for removing batch effects and other unwanted variation in high-throughput experiments. Bioinformatics 28:882–883.
[38] Dobin, A., Davis, C.A., Schlesinger, F., Drenkow, J., Zaleski, C., Jha, S., et al., 2013. STAR: ultrafast universal RNA-seq aligner. Bioinformatics 29:15–21.
[39] Kim, D., Langmead, B., Salzberg, S.L., 2015. HISAT: a fast spliced aligner with low memory requirements. Nature Methods 12:357–360.
[40] Love, M.I., Anders, S., Kim, V., Huber, W., 2015. RNA-Seq workflow: gene-level exploratory analysis and differential expression. F1000Res 4:1070.
[41] Benjamini, Y., Hochberg, Y., 1995. Controlling the false discovery rate – a practical and powerful approach to multiple testing. Journal of the Royal Statistical Society – Series B: Statistical Methodology 57:289–300.
[42] Langfelder, P., Horvath, S., 2008. WGCNA: an R package for weighted correlation network analysis. BMC Bioinformatics 9:559.
[43] Seldin, M.M., Koplev, S., Rajbhandari, P., Vergnes, L., Rosenberg, G.M., Meng, Y., et al., 2018. A strategy for discovery of endocrine interactions with application to whole-body metabolism. Cell Metabolism 27:1138–1155 e6.
[44] O'Neill, S.M., Hinkle, C., Chen, S.J., Sandhu, A., Hovhannisyan, R., Stephan, S., et al., 2014. Targeting adipose tissue via systemic gene therapy. Gene Therapy 21:653–661.
[45] Knott, S.R.V., Maceli, A., Erard, N., Chang, K., Marran, K., Zhou, X., et al., 2014. A computational algorithm to predict shRNA potency. Molecular Cell 56:796–807.
[46] Fellmann, C., Hoffmann, T., Sridhar, V., Hopfgartner, B., Muhar, M., Roth, M., et al., 2013. An optimized microRNA backbone for effective single-copy RNAi. Cell Reports 5:1704–1713.
[47] Folch, J., Lees, M., Sloane Stanley, G.H., 1957. A simple method for the isolation and purification of total lipides from animal tissues. Journal of Biological Chemistry 226:497–509.
[48] Han, S., Bahmanyar, S., Zhang, P., Grishin, N., Oegema, K., Crooke, R., et al., 2012. Nuclear envelope phosphatase 1-regulatory subunit 1 (formerly TMEM188) is the metazoan Spo7p ortholog and functions in the lipin activation pathway. Journal of Biological Chemistry 287:3123–3137.
[49] Vandesompele, J., De Preter, K., Pattyn, F., Poppe, B., Van Roy, N., De Paepe, A., et al., 2002. Accurate normalization of real-time quantitative RT-PCR data by geometric averaging of multiple internal control genes. Genome Biology 3. RESEARCH0034.
[50] Vergnes, L., Chin, R., Young, S.G., Reue, K., 2011. Heart-type fatty acid-binding protein is essential for efficient brown adipose tissue fatty acid oxidation and cold tolerance. Journal of Biological Chemistry 286:380–390.
[51] Rooney, J.P., Ryde, I.T., Sanders, L.H., Howlett, E.H., Colton, M.D., Germ, K.E., et al., 2015. PCR based determination of mitochondrial DNA copy number in multiple species. Methods in Molecular Biology 1241:23–38.
[52] Venegas, V., Halberg, M.C., 2012. Measurement of mitochondrial DNA copy number. Methods in Molecular Biology 837:327–335.
[53] Rogers, G.W., Brand, M.D., Petrosyan, S., Ashok, D., Elorza, A.A., Ferrick, D.A., et al., 2011. High throughput microplate respiratory measurements using minimal quantities of isolated mitochondria. PLoS One 6: e21746.
[54] Wu, M., Neilson, A., Swift, A.L., Moran, R., Tamagnine, J., Parslow, D., et al., 2007. Multiparameter metabolic analysis reveals a close link between attenuated mitochondrial bioenergetic function and enhanced glycolysis dependency in human tumor cells. American Journal of Physiology – Cell Physiology 292:C125–C136.
[55] Khor, V.K., Tong, M.H., Qian, Y., Song, W.C., 2008. Gender-specific expression and mechanism of regulation of estrogen sulfotransferase in adipose tissues of the mouse. Endocrinology 149:5440–5448.
[56] Norheim, F., Hasin-Brumshtein, Y., Vergnes, L., Chella Krishnan, K., Pan, C., Seldin, M.M., et al., 2019. Gene-by-Sex interactions in mitochondrial functions and cardio-metabolic traits. Cell Metabolism 29:932–949 e4.

[57] Nookaew, I., Svensson, P.A., Jacobson, P., Jernas, M., Taube, M., Larsson, I., et al., 2013. Adipose tissue resting energy expenditure and expression of genes involved in mitochondrial function are higher in women than in men. The Journal of Clinical Endocrinology & Metabolism 98:E370–E378.

[58] Kim, S.N., Jung, Y.S., Kwon, H.J., Seong, J.K., Granneman, J.G., Lee, Y.H., 2016. Sex differences in sympathetic innervation and browning of white adipose tissue of mice. Biology of Sex Differences 7:67.

[59] Donkor, J., Sariahmetoglu, M., Dewald, J., Brindley, D.N., Reue, K., 2007. Three mammalian lipins act as phosphatidate phosphatases with distinct tissue expression patterns. Journal of Biological Chemistry 282:3450–3457.

[60] Reue, K., Xu, P., Wang, X.P., Slavin, B.G., 2000. Adipose tissue deficiency, glucose intolerance, and increased atherosclerosis result from mutation in the mouse fatty liver dystrophy (fld) gene. The Journal of Lipid Research 41: 1067–1076.

[61] Peterfy, M., Phan, J., Reue, K., 2005. Alternatively spliced lipin isoforms exhibit distinct expression pattern, subcellular localization, and role in adipogenesis. Journal of Biological Chemistry 280:32883–32889.

[62] Koh, Y.K., Lee, M.Y., Kim, J.W., Kim, M., Moon, J.S., Lee, Y.J., et al., 2008. Lipin1 is a key factor for the maturation and maintenance of adipocytes in the regulatory network with CCAAT/enhancer-binding protein alpha and peroxisome proliferator-activated receptor gamma 2. Journal of Biological Chemistry 283:34896–34906.

[63] Kim, H.B., Kumar, A., Wang, L., Liu, G.H., Keller, S.R., Lawrence Jr., J.C., et al., 2010. Lipin 1 represses NFATc4 transcriptional activity in adipocytes to inhibit secretion of inflammatory factors. Molecular and Cellular Biology 30: 3126–3139.

[64] Nakai, H., Fuess, S., Storm, T.A., Muramatsu, S., Nara, Y., Kay, M.A., 2005. Unrestricted hepatocyte transduction with adeno-associated virus serotype 8 vectors in mice. Journal of Virology 79:214–224.

[65] Song, E., Fan, P., Huang, B., Deng, H.B., Cheung, B.M., Feletou, M., et al., 2014. Deamidated lipocalin-2 induces endothelial dysfunction and hypertension in dietary obese mice. Journal of the American Heart Association 3: e000837.

[66] Yang, K., Deng, H.B., Man, A.W.C., Song, E., Zhang, J., Luo, C., et al., 2017. Measuring non-polyaminated lipocalin-2 for cardiometabolic risk assessment. ESC Heart Failure 4:563–575.

[67] Sun, W.Y., Bai, B., Luo, C., Yang, K., Li, D., Wu, D., et al., 2018. Lipocalin-2 derived from adipose tissue mediates aldosterone-induced renal injury. JCI Insight 3.

[68] Azimifar, S.B., Nagaraj, N., Cox, J., Mann, M., 2014. Cell-type-resolved quantitative proteomics of murine liver. Cell Metabolism 20:1076–1087.

[69] Huang, da W., Sherman, B.T., Lempicki, R.A., 2009. Systematic and integrative analysis of large gene lists using DAVID bioinformatics resources. Nature Protocols 4:44–57.

[70] Chen, J., Bardes, E.E., Aronow, B.J., Jegga, A.G., 2009. ToppGene Suite for gene list enrichment analysis and candidate gene prioritization. Nucleic Acids Research 37:W305–W311.

[71] Sun, K., Halberg, N., Khan, M., Magalang, U.J., Scherer, P.E., 2013. Selective inhibition of hypoxia-inducible factor 1alpha ameliorates adipose tissue dysfunction. Molecular and Cellular Biology 33:904–917.

[72] Guglielmi, V., Cardellini, M., Cinti, F., Corgosinho, F., Cardolini, I., D'Adamo, M., et al., 2015. Omental adipose tissue fibrosis and insulin resistance in severe obesity. Nutrition & Diabetes 5:e175.

[73] Khan, T., Muise, E.S., Iyengar, P., Wang, Z.V., Chandalia, M., Abate, N., et al., 2009. Metabolic dysregulation and adipose tissue fibrosis: role of collagen VI. Molecular and Cellular Biology 29:1575–1591.

[74] Pasarica, M., Gowronska-Kozak, B., Burk, D., Remedios, I., Hymel, D., Gimble, J., et al., 2009. Adipose tissue collagen VI in obesity. The Journal of Clinical Endocrinology & Metabolism 94:5155–5162.

[75] Kanda, H., Tateya, S., Tamori, Y., Kotani, K., Hiasa, K., Kitazawa, R., et al., 2006. MCP-1 contributes to macrophage infiltration into adipose tissue, insulin resistance, and hepatic steatosis in obesity. Journal of Clinical Investigation 116:1494–1505.

[76] Sekimoto, R., Fukuda, S., Maeda, N., Tsushima, Y., Matsuda, K., Mori, T., et al., 2015. Visualized macrophage dynamics and significance of S100A8 in obese fat. Proceedings of the National Academy of Sciences of the United States of America 112:E2058–E2066.

[77] Sanada, Y., Yamamoto, T., Satake, R., Yamashita, A., Kanai, S., Kato, N., et al., 2016. Serum amyloid A3 gene expression in adipocytes is an indicator of the interaction with macrophages. Scientific Reports 6:38697.

[78] Buscher, K., Ehinger, E., Gupta, P., Pramod, A.B., Wolf, D., Tweet, G., et al., 2017. Natural variation of macrophage activation as disease-relevant phenotype predictive of inflammation and cancer survival. Nature Communications 8:16041.

[79] Devireddy, L.R., Gazin, C., Zhu, X., Green, M.R., 2005. A cell-surface receptor for lipocalin 24p3 selectively mediates apoptosis and iron uptake. Cell 123: 1293–1305.

[80] Hvidberg, V., Jacobsen, C., Strong, R.K., Cowland, J.B., Moestrup, S.K., Borregaard, N., 2005. The endocytic receptor megalin binds the iron transporting neutrophil-gelatinase-associated lipocalin with high affinity and mediates its cellular uptake. FEBS Letters 579:773–777.

[81] Zhang, Y., Guo, H., Deis, J.A., Mashek, M.G., Zhao, M., Ariyakumar, D., et al., 2014. Lipocalin 2 regulates brown fat activation via a nonadrenergic activation mechanism. Journal of Biological Chemistry 289:22063–22077.

[82] Deis, J.A., Guo, H., Wu, Y., Liu, C., Bernlohr, D.A., Chen, X., 2019. Adipose Lipocalin 2 overexpression protects against age-related decline in thermogenic function of adipose tissue and metabolic deterioration. Molecular Metabolism 24:18–29.

[83] Slattery, M.J., Bredella, M.A., Thakur, H., Torriani, M., Misra, M., 2014. Insulin resistance and impaired mitochondrial function in obese adolescent girls. Metabolic Syndrome and Related Disorders 12:56–61.

[84] Zamora-Mendoza, R., Rosas-Vargas, H., Ramos-Cervantes, M.T., Garcia-Zuniga, P., Perez-Lorenzana, H., Mendoza-Lorenzo, P., et al., 2018. Dysregulation of mitochondrial function and biogenesis modulators in adipose tissue of obese children. International Journal of Obesity (Lond) 42:618–624.

[85] Lahera, V., de Las Heras, N., Lopez-Farre, A., Manucha, W., Ferder, L., 2017. Role of mitochondrial dysfunction in hypertension and obesity. Current Hypertension Reports 19:11.

[86] Wilson-Fritch, L., Nicoloro, S., Chouinard, M., Lazar, M.A., Chui, P.C., Leszyk, J., et al., 2004. Mitochondrial remodeling in adipose tissue associated with obesity and treatment with rosiglitazone. Journal of Clinical Investigation 114:1281–1289.

[87] Choo, H.J., Kim, J.H., Kwon, O.B., Lee, C.S., Mun, J.Y., Han, S.S., et al., 2006. Mitochondria are impaired in the adipocytes of type 2 diabetic mice. Diabetologia 49:784–791.

[88] Rong, J.X., Qiu, Y., Hansen, M.K., Zhu, L., Zhang, V., Xie, M., et al., 2007. Adipose mitochondrial biogenesis is suppressed in db/db and high-fat diet-fed mice and improved by rosiglitazone. Diabetes 56:1751–1760.

[89] Alwahsh, S.M., Xu, M., Seyhan, H.A., Ahmad, S., Mihm, S., Ramadori, G., et al., 2014. Diet high in fructose leads to an overexpression of lipocalin-2 in rat fatty liver. World Journal of Gastroenterology 20:1807–1821.

[90] Asimakopoulou, A., Fulop, A., Borkham-Kamphorst, E., de Leur, E.V., Gassler, N., Berger, T., et al., 2017. Altered mitochondrial and peroxisomal integrity in lipocalin-2-deficient mice with hepatic steatosis. Biochimica et Biophysica Acta – Molecular Basis of Disease 1863:2093–2110.

[91] Song, E., Ramos, S.V., Huang, X., Liu, Y., Botta, A., Sung, H.K., et al., 2018. Holo-lipocalin-2-derived siderophores increase mitochondrial ROS and impair oxidative phosphorylation in rat cardiomyocytes. Proceedings of the National Academy of Sciences of the United States of America 115:1576–1581.

[92] Xu, G., Ahn, J., Chang, S., Eguchi, M., Ogier, A., Han, S., et al., 2012. Lipocalin-2 induces cardiomyocyte apoptosis by increasing intracellular iron accumulation. Journal of Biological Chemistry 287:4808–4817.

[93] Chan, Y.K., Sung, H.K., Sweeney, G., 2015. Iron metabolism and regulation by neutrophil gelatinase-associated lipocalin in cardiomyopathy. Clinical Science (Lond) 129:851–862.

[94] Klinge, C.M., 2008. Estrogenic control of mitochondrial function and biogenesis. Journal of Cellular Biochemistry 105:1342–1351.

[95] Ribas, V., Drew, B.G., Zhou, Z., Phun, J., Kalajian, N.Y., Soleymani, T., et al., 2016. Skeletal muscle action of estrogen receptor alpha is critical for the maintenance of mitochondrial function and metabolic homeostasis in females. Science Translational Medicine 8:334ra54.

[96] Lumeng, C.N., Saltiel, A.R., 2011. Inflammatory links between obesity and metabolic disease. Journal of Clinical Investigation 121:2111–2117.

[97] Marzolo, M.P., Farfan, P., 2011. New insights into the roles of megalin/LRP2 and the regulation of its functional expression. Biological Research 44:89–105.

[98] Hammes, A., Andreassen, T.K., Spoelgen, R., Raila, J., Hubner, N., Schulz, H., et al., 2005. Role of endocytosis in cellular uptake of sex steroids. Cell 122:751–762.

[99] Abboud, M., Gordon-Thomson, C., Hoy, A.J., Balaban, S., Rybchyn, M.S., Cole, L., et al., 2014. Uptake of 25-hydroxyvitamin D by muscle and fat cells. The Journal of Steroid Biochemistry and Molecular Biology 144(Pt A):232–236.

[100] Bonnet, L., Karkeni, E., Couturier, C., Astier, J., Dalifard, J., Defoort, C., et al., 2018. Gene expression pattern in response to cholecalciferol supplementation highlights cubilin as a major protein of 25(OH)D uptake in adipocytes and male mice white adipose tissue. Endocrinology 159:957–966.

[101] Yiannikouris, F., Wang, Y., Shoemaker, R., Larian, N., Thompson, J., English, V.L., et al., 2015. Deficiency of angiotensinogen in hepatocytes markedly decreases blood pressure in lean and obese male mice. Hypertension 66:836–842.

